Cell Reports

Article

Dorsal BNST DRD2$^+$ neurons mediate sex-specific anxiety-like behavior induced by chronic social isolation

Graphical abstract

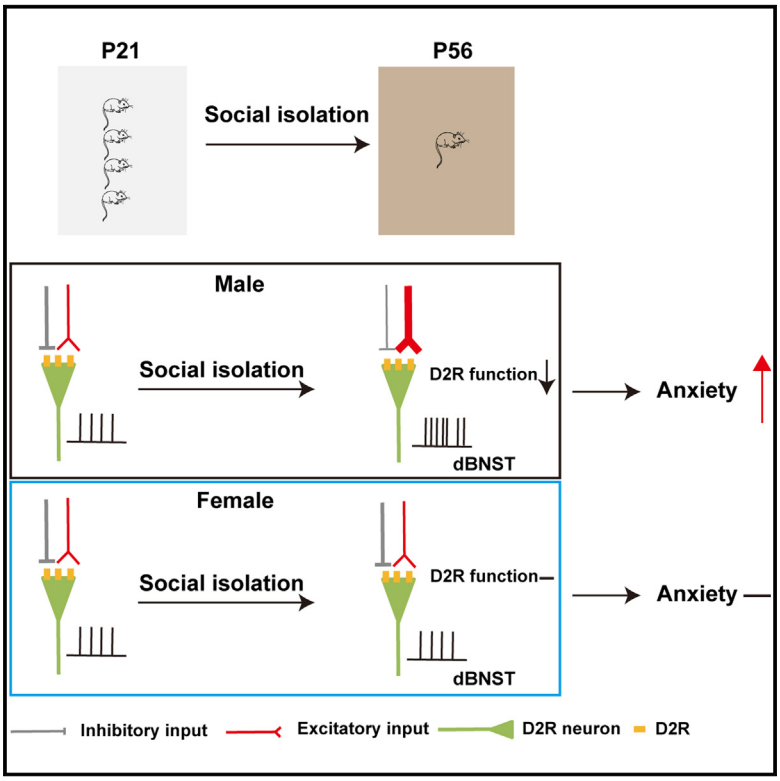

Highlights

- PWSI stress induces male-specific emotional and social dysfunction
- Excitability of dBNST Drd2$^+$, but not Drd1$^+$, neurons of PWSI rats shows an increase
- There is an enhancement of E:I balance of dBNST Drd2$^+$ neurons in PWSI rats
- Inhibition of dBNST Drd2$^+$ neurons rescues anxiety-like phenotype caused by PWSI stress

Authors

Chaowen Zheng, Lei Wei, Boyi Liu, ..., Xiangning Li, Hui Gong, Zuoren Wang

Correspondence

zuorenwang@ion.ac.cn

In brief

Zheng et al. find an important mechanism by which post-weaning social isolation stress induces male-specific anxiety-like behavior by the increase of the excitability of dBNST Drd2$^+$, but not Drd1$^+$, neurons and enhancement of E:I balance of dBNST Drd2$^+$ neurons.

Zheng et al., 2023, Cell Reports *42*, 112799
July 25, 2023
https://doi.org/10.1016/j.celrep.2023.112799

CellPress

Cell Reports

CellPress
OPEN ACCESS

Article

Dorsal BNST DRD2$^+$ neurons mediate sex-specific anxiety-like behavior induced by chronic social isolation

Chaowen Zheng,[1,2,6,7] Lei Wei,[1,7] Boyi Liu,[1,2,7] Qingxiu Wang,[1] Yanwang Huang,[1,2] Shangyi Wang,[1,2,3] Xiangning Li,[4] Hui Gong,[4,5] and Zuoren Wang[1,2,3,8,*]

[1]Institute of Neuroscience, State Key Laboratory of Neuroscience, CAS Center for Excellence in Brain Science and Intelligence Technology, Chinese Academy of Sciences, Shanghai 200031, China
[2]University of Chinese Academy of Sciences, Beijing 100049, China
[3]School of Future Technology, University of Chinese Academy of Sciences, Beijing 100049, China
[4]Research Unit of Multimodal Cross Scale Neural Signal Detection and Imaging, Chinese Academy of Medical Sciences, HUST-Suzhou Institute for Brainsmatics, JITRI, Suzhou 215000, China
[5]CAS Center for Excellence in Brain Science and Intelligence Technology, Chinese Academy of Science, Shanghai 200031, China
[6]Neuroscience Research Center, Institute of Mitochondrial Biology and Medicine, Key Laboratory of Biomedical Information Engineering of Ministry of Education, School of Life Science and Technology and Core Facilities Sharing Platform, Xi'an Jiaotong University, Xi'an 710049, China
[7]These authors contributed equally
[8]Lead contact
*Correspondence: zuorenwang@ion.ac.cn
https://doi.org/10.1016/j.celrep.2023.112799

SUMMARY

The dorsal bed nucleus of stria terminalis (dBNST) is a pivotal hub for stress response modulation. Dysfunction of dopamine (DA) network is associated with chronic stress, but the roles of DA network of dBNST in chronic stress-induced emotional disorders remain unclear. We examine the role of dBNST Drd1$^+$ and Drd2$^+$ neurons in post-weaning social isolation (PWSI)-induced behavior deficits. We find that male, but not female, PWSI rats exhibit negative emotional phenotypes and the increase of excitability and E-I balance of dBNST Drd2$^+$ neurons. More importantly, hypofunction of dBNST Drd2 receptor underlies PWSI-stress-induced male-specific neuronal plasticity change of dBNST Drd2$^+$ neurons. Furthermore, chemogenetic activation of dBNST Drd2$^+$ neurons is sufficient to induce anxiogenic effects, while Kir4.1-mediated chronic inhibition of dBNST Drd2$^+$ neurons ameliorate PWSI-induced anxiety-like behaviors. Our findings reveal an important neural mechanism underlying PWSI-induced sex-specific behavioral abnormalities and potentially provide a target for the treatment of social stress-related emotional disorder.

INTRODUCTION

Social stimuli, especially during adolescence, are critical for the establishment of normal emotional states and cognitive function in adulthood.[1,2] As an early-life stress, social isolation or deprivation during adolescence can heighten vulnerability to anxiety, social deficits, and cognitive impairments.[3–5] Studies using different models of social isolation during adolescence in rodents have demonstrated that socially isolated animals develop behavioral abnormalities in adulthood, which includes attention deficits, hyperactivity, anxiety-like behavior, and social deficits.[6–10] However, the cellular mechanisms through which social isolation in adolescence triggers these behavioral abnormalities in adulthood remain unclear. Therefore, it is of great importance to identify the underlying neural substrates, which may shed light on the treatment of mental illnesses caused by social isolation and other stressors as well.

It has been reported that dopamine (DA) systems play a key role in regulating emotion, cognition, and social reward.[11,12] Rodents that have experienced social isolation in adolescence exhibit dysfunction in their DA systems.[13,14] For instance, DA turnover is altered in the hippocampus and ventral striatum, and the affinity of DA receptor 2 (Drd2) is changed in the striatum in chronic socially isolated animals.[6,15] However, the molecular and circuit mechanisms of the DA system involved in the affective and social disorders induced by chronic social isolation stress remain unclear.

The dorsal part of the bed nucleus of the stria terminalis (dBNST), which includes the anterior dBNST (adBNST) and oval BNST (ovBNST), is termed the extended amygdala. It has been reported that the dBNST is a critical nucleus in integrating negative values, and regulating negative emotions and stress responses.[16,17] Many subregions are included,[18,19] and a variety of hormones and peptide receptors are expressed in this brain

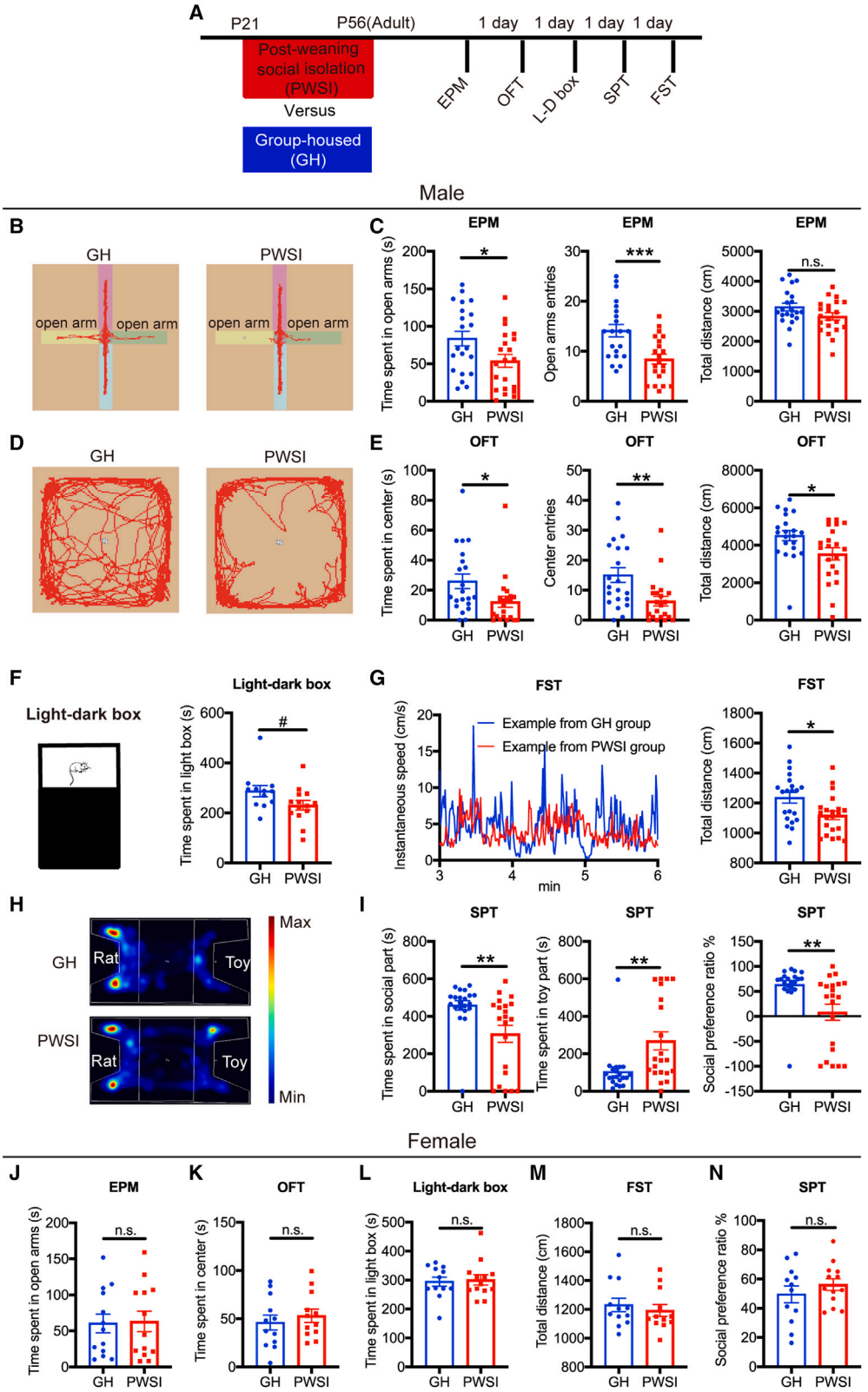

(legend on next page)

region.[20–22] Thus, the anatomical organization and physiological function of the dBNST remain unclear. Previous studies have shown that the dBNST receives dopaminergic inputs from different upstream sources.[23,24] However, the physiological functions of the dopaminergic synaptic transmission in the dBNST remain unclear.

In the current study, using a post-weaning social isolation (PWSI) rat model, we examined whether dBNST neurons expressing DA receptors (DA receptor type 1 or 2; Drd1 or Drd2, respectively) are involved in PWSI-induced behavioral abnormalities. First, we found that male, but not female, PWSI rats exhibited excessive maladaptive avoidance behavioral phenotypes, as well as an associated increase in neuronal excitability and net excitatory input of dBNST Drd2$^+$ neurons. More importantly, we found that the male-specific impairment of dBNST Drd2 receptors underlies the PWSI-induced sex-specific neuronal excitability change. Furthermore, we manipulated the activity of dBNST Drd2$^+$ neurons and demonstrated causality between increased activity of dBNST Drd2$^+$ neurons and the level of anxiety-like behaviors of PWSI male rats. Taken together, our findings demonstrate that hyperactivity of Drd2$^+$ neurons in the dBNST is a key mechanism underlying PWSI-induced sex-specific anxiety-like behaviors.

RESULTS

Male, but not female, rats developed excessive maladaptive avoidance behaviors after PWSI stress

To dissect the underlying neural mechanism of social stress-induced mental disorders, we first established a rat model of PWSI, and a battery of behavioral tests were performed to assess the influence of PWSI stress on their emotional states and sociality (Figure 1A). The results showed that, compared with group-housed (GH) male rats, PWSI male rats exhibited less exploratory motivation in the open arms in the elevated plus maze (EPM) and the central region in the open field test (OFT) (Figures 1B–1E). In addition, we found that PWSI male rats spent less time in the light box during the light-dark (L-D) box test (Figure 1F). Together, these results demonstrated that PWSI male rats developed anxiety-like phenotypes. We also found that PWSI male rats exhibited less struggling in the forced swim test (FST), as suggested by the total distance that rats swam (Figure 1G). Furthermore, we found that PWSI male rats showed decreased social preference to conspecifics than GH rats did (Figures 1H and 1I), demonstrating that PWSI male rats developed social deficits in adulthood. Parallel with the changes in behavioral performance, the level of stress hormone corticosterone also significantly increased in PWSI male rats (Figures S1A and S1B). Taken together, these results revealed that PWSI male rats developed excessive maladaptive avoidance behaviors, which include the avoidance of exposure to an open context, active coping, and social interaction. Interestingly, when isolated in adulthood (P56-P91), male rats did not display the phenotype exhibited in PWSI rats (Figure S2). Thus, these results indicated the post-weaning period is the critical window for social isolation-induced excessive maladaptive avoidance behavior. Furthermore, we found that PWSI female rats also did not show a significant behavioral phenotype in the EPM, OFT, L-D box, FST, and social preference test (SPT) (Figures 1J–1N), and the corticosterone level only showed a slight but not significant tendency of increase (Figure S1C). Furthermore, we found that the interaction effects between housing condition (GH vs. PWSI) and sex (male vs. female) have the tendency to become statistically significant (Figure S3), these results indicate that the effects of PWSI stress are sex specific.

PWSI stress affects the neuronal excitability of Drd2$^+$ neurons in dBNST in a sex-specific manner

To explore the role of the dBNST in PWSI-induced behavioral abnormality, we first examined whether the excitability of dBNST neurons was changed in PWSI male rats using a whole-cell patch-clamp recording technique (Figures S4A and S4B). We found that the resting membrane potential and input resistance of dBNST neurons were comparable between PWSI and GH rats (Figures S4C and S4D). For the neuronal responses to

Figure 1. Sex-dependent influence of PWSI stress on behavioral phenotypes of rats

(A) Timeline showing the procedures of PWSI modeling and behavioral tests of socially isolated (PWSI group) or group-housed (GH group) rats.

(B) Examples of the locomotion trajectory of male rats from GH and PWSI groups in the EPM test.

(C) Comparison of time spent in the open arms (left), number of open arm entries (middle), and total distance (right) that male rats moved in the EPM test from GH and PWSI groups (Student's t test, left, $p = 0.0282$; middle, $p = 0.0009$; right, $p = 0.0833$).

(D) Examples of the locomotion trajectory of male rats from GH and PWSI groups in the OFT.

(E) Comparison of the time that male rats from GH and PWSI groups spent in the center (left), number of center entries (middle), and total distance that rats moved in the OFT (right) (Student's t test, left, $p = 0.0297$; middle, $p = 0.0049$; right, $p = 0.0265$).

(F) Left: Schematic diagram of L-D box test. Right: Comparison of time spent in the light box in the L-D box test by male GH and PWSI rats (Mann-Whitney *U* test, $p = 0.0407$).

(G) Left: Examples of instantaneous swimming velocity of two male rats from GH and PWSI groups in FST; Right: Comparison of swimming distance of male rats from GH and PWSI groups in the FST (Student's t test, $p = 0.0144$).

(H) Examples of the heatmap of the locomotion trajectory of male rats from GH and PWSI groups in the SPT.

(I) Comparison of time spent in the social part (left, Student's t test, $p = 0.0054$), time spent in the toy part (middle, Student's t test, $p = 0.0044$), and social preference ratio (right, Mann-Whitney *U* test, $p = 0.0024$) of male rats from GH and PWSI groups.

(J) Comparison of time spent in the open arms in the EPM test of female rats from the GH and PWSI groups (Student's t test, $p = 0.89$).

(K) Comparison of time that female rats from the GH and PWSI groups spent in the center in the OFT (Student's t test, $p = 0.49$).

(L) Comparison of the time spent in the light box in the L-D box test of female GH and PWSI rats (Mann-Whitney *U* test, $p = 0.65$).

(M) Comparison of the swimming distance of female rats from the GH and PWSI groups in the FST (Student's t test, $p = 0.55$).

(N) Comparison of the social preference ratio (Student's t test, $p = 0.34$) of female rats from the GH and PWSI groups. Data are shown as mean ± SEM. $^*p < 0.05$, $^{**}p < 0.01$, $^{***}p < 0.001$, Student's t test. n.s., not significant. #$p < 0.05$, Mann-Whitney *U* test.

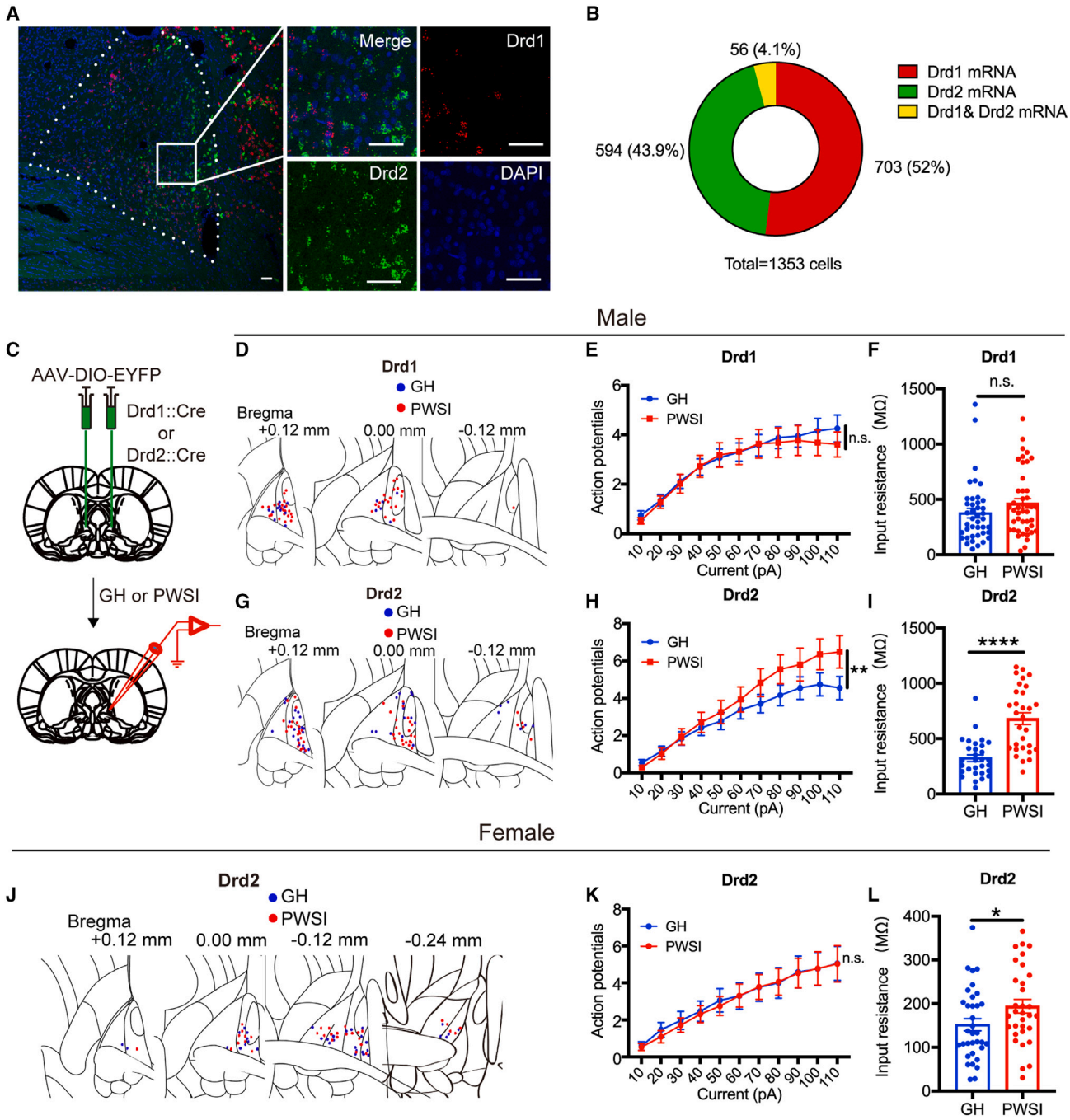

Figure 2. Sex-dependent influence of PWSI stress on neuronal plasticity change of dBNST Drd2$^+$ neurons

(A) Expression pattern of Drd1 and Drd2 mRNA in dBNST; left panel represents the distribution of these two mRNAs in the dBNST; right panels are the enlargements of the windowed area in the left panel, including merged image, expression patterns of Drd1 mRNA, Drd2 mRNA, and DAPI staining. Magnification folds, 3. Scale bar represents 50 μm.

(B) Statistics of distribution of Drd1 and Drd2 mRNA expression in dBNST neurons.

(C) Schematic diagrams show the procedures of Drd1$^+$and Drd2$^+$ neuron labeling (top) and patch-clamp recording (bottom).

(D) Schematic of the recording sites of Drd1$^+$ neurons in dBNST of male rats from GH and PWSI groups.

(E) Comparison of step current-induced action potential numbers of dBNST Drd1$^+$ neurons of male rats from GH and PWSI groups (two-way RM ANOVA, housing [GH vs. PWSI] × step current interaction: $F_{10,935} = 0.1403$, $p = 0.9992$; step current: $F_{10,935} = 13.44$, $p < 0.0001$; housing: $F_{1,935} = 0.6710$, $p = 0.4129$).

(F) Comparison of input resistance of dBNST Drd1$^+$ neurons of male rats from GH and PWSI groups (Student's t test, $p = 0.1486$).

(G) Schematic of the recording sites of Drd2$^+$ neurons in the dBNST of male rats from GH and PWSI groups.

(legend continued on next page)

step-current injection, the action potential numbers were significantly increased in the PWSI group (Figures S4E and S4F), indicating that the excitability of dBNST neurons was increased in PWSI rats.

Evidence has shown that DA receptors, especially the D2 receptor, regulate the emotional state in the brain.[25] Furthermore, DA receptors are targets of antipsychotic drugs.[26] Thus, we asked whether the excitability of DA receptor-positive neurons in the dBNST was changed after PWSI stress. First, we examined the distribution of two major receptors of DA systems—Drd1 and Drd2 receptors—in the dBNST using the RNAscope technique. The results showed that these two receptors were separately expressed in different subsets of neurons in the dBNST (Figures 2A and 2B). Inconsistent with previous studies on mice,[27] our *in situ* hybridization results showed that Drd1 mRNA in Sprague Dawley (SD) rats are predominantly expressed in the anterior (adBNST) but not the oval part of the dBNST, whereas Drd2 mRNA is evenly expressed in both regions (Figures S5A and S5B). This inconsistency may attribute to the difference of animal species.

After verifying the specificity of Drd1::Cre and Drd2::Cre transgenic rats and Cre recombinase-dependent expression of AAV-DIO-EYFP in Drd1$^+$ and Drd2$^+$ neurons of the dBNST (Figures S5C–S5F), we examined the electrophysiological properties of Drd1$^+$ and Drd2$^+$ neurons. According to the classification criteria described in "Electrophysiology," we found that both Drd1$^+$ and Drd2$^+$ neurons were composed of neuron types with different electrophysiological properties, including low-threshold bursting (LTB), regular spiking (RS), fast inward rectifying K^+ conductance (fIR), and spontaneous activity (SA; Figures S6A and S6B). Thus, both Drd1$^+$ and Drd2$^+$ neurons in the dBNST are heterogeneous in terms of electrophysiological properties.

Since PWSI stress affects the behavior and the global neuronal excitability in the dBNST of male rats, we next examined the influence of PWSI stress on the excitability of Drd1$^+$ and Drd2$^+$ neurons in the dBNST of male rats. As shown in Figures S7A, S7B, and 2C–2F, the membrane potential, action potential threshold, current injection-induced action potential numbers, and input resistance of Drd1$^+$ neurons in the dBNST were comparable between GH and PWSI male rats. Notably, even though the membrane potential and action potential threshold were comparable between the GH and PWSI groups (Figures S7C and S7D), the current injection-induced action potential numbers and input resistance of Drd2$^+$ neurons were significantly increased in PWSI rats (Figures 2G–2I), indicating that the excitability of dBNST Drd2$^+$ but not Drd1$^+$ neurons was specifically increased in PWSI male rats.

In parallel, we also measured the excitability of dBNST Drd2$^+$ neurons in GH and PWSI female rats. The results showed that the current injection-induced action potential numbers were comparable between GH and PWSI rats (Figures 2J and 2K). Although the resting membrane potential was decreased and the input resistance was increased in the PWSI group, the effect was very slight (Figures 2J, 2L, S8A, and S8B). Together, these results suggested that the effect of PWSI stress on the excitability of dBNST Drd2$^+$ neurons is associated with PWSI-induced behavior deficits in a sex-specific manner.

The net excitatory input is specifically increased in dBNST Drd2$^+$ but not Drd1$^+$ neurons of PWSI male rats

Our results demonstrated that the increase in the excitability of dBNST Drd2$^+$ neurons was sex-specifically associated with the behavioral deficits of PWSI male rats. We next examined whether their excitatory and inhibitory inputs were also changed. We found that neither the frequency nor the amplitude of the miniature excitatory postsynaptic currents (mEPSCs) of dBNST Drd1$^+$ neurons showed a significant difference between GH and PWSI rats (Figures 3A–3D). For the results of miniature inhibitory postsynaptic currents (mIPSCs), even though the mIPSCs frequency of dBNST Drd1$^+$ neurons showed a slight tendency of decrease ($p = 0.083$), the amplitude of mIPSCs was comparable between GH and PWSI rats (Figures 3E–3H). However, in contrast to Drd1$^+$ neurons, the frequency but not the amplitude, of mEPSCs of dBNST Drd2$^+$ neurons was significantly increased in PWSI male rats (Figures 3I–3L). Furthermore, the frequency, but not the amplitude, of mIPSCs of dBNST Drd2$^+$ neurons was significantly decreased in PWSI male rats (Figures 3M–3P). Notably, we found that when compared with the results of female GH rats, both the frequency and amplitude of the mEPSCs and mIPSCs of dBNST Drd2$^+$ neurons of female PWSI rats do not show a significant difference (Figure S9). These results demonstrate that, in addition to the increase in excitability of dBNST Drd2$^+$ neurons, the net excitatory input of dBNST Drd2$^+$ but not Drd1$^+$ neurons was also specifically increased in PWSI male rats.

To investigate the upstream input of dBNST Drd1$^+$ and Drd2$^+$ neurons, mono-synaptic retrograde tracing by a strategy of rabies virus was conducted to dissect the afferents of dBNST Drd1$^+$ and Drd2$^+$ neurons. In brief, the Cre recombinase-dependent AAV-FLEX-mCherry-2A-TVA-2A-RvG, which encodes avian retroviral receptor (TVA) and glycoprotein of rabies virus (RvG), was first unilaterally injected into the dBNST of Drd1::Cre and Drd2::Cre male rats, and then the TVA-deficient EnvA-pseudotyped rabies virus RV-ENVA-ΔG-EGFP was expressed into the dBNST (Figure 3Q). The results revealed distinct distribution patterns of retrograde-labeled EGFP$^+$ neurons (Drd1, Figure 3R; Drd2, Figure 3S). We also found that both the dBNST Drd1$^+$ and Drd2$^+$ neurons receive inputs from dBNST

(H) Comparison of step current-induced action potential numbers of dBNST Drd2$^+$ neurons of male rats from GH and PWSI groups (two-way RM ANOVA, housing [GH vs. PWSI] × step current interaction: $F_{10,968} = 0.5351$, $p = 0.8660$; step current: $F_{10,968} = 25.09$, $p < 0.0001$; housing: $F_{1,968} = 11.58$, $p = 0.0007$).
(I) Comparison of input resistance of dBNST Drd2$^+$ neurons of male rats from GH and PWSI groups (Student's t test, $p < 0.0001$).
(J) Schematic of the recording sites of Drd2$^+$ neurons in the dBNST of female rats from GH and PWSI groups.
(K) Comparison of step current-induced action potential numbers of dBNST Drd2$^+$ neurons of female rats from GH and PWSI groups (two-way RM ANOVA, housing (GH vs. PWSI) × step current interaction: $F_{10,704} = 0.02474$, $p > 0.9999$; step current: $F_{10,704} = 9.726$, $p < 0.0001$; housing: $F_{1,704} = 0.1271$, $p = 0.7215$).
(L) Comparison of input resistance of dBNST Drd2$^+$ neurons of female rats from GH and PWSI groups (Student's t test, $p = 0.0471$). Data are shown as mean ± SEM. *$p < 0.05$, **$p < 0.01$, ****$p < 0.0001$.; n.s., not significant.

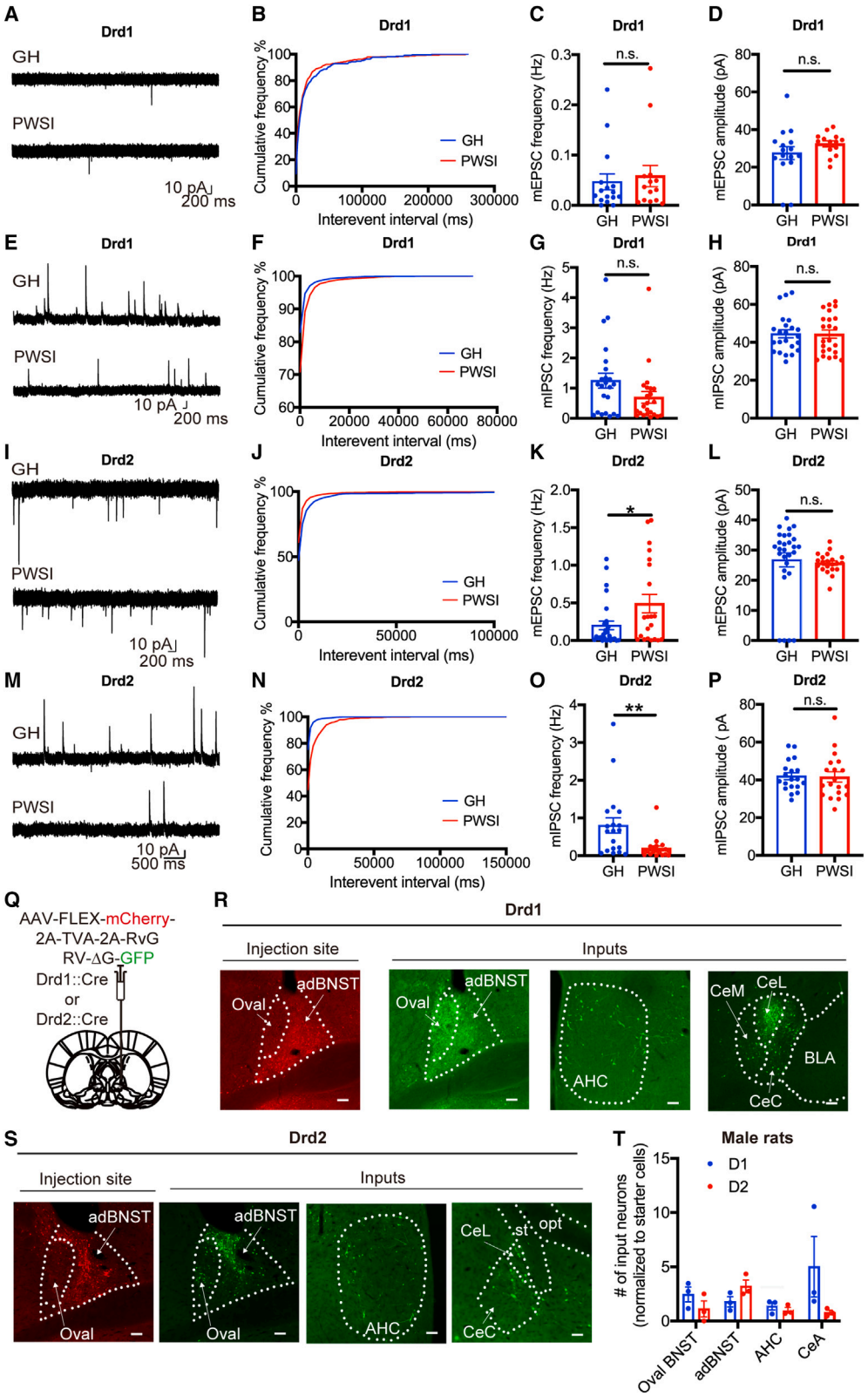

(legend on next page)

(oval BNST and adBNST), anterior hypothalamus central area (AHC), and the central amygdala (CeA) (Figure 3T).

The excitability of dBNST Drd2$^+$ neurons is positively correlated with the level of anxiety-like phenotype in animals

To further investigate the relationship between the excitability of Drd2$^+$ neurons and PWSI-induced phenotypes, we examined the correlation between the level of specific phenotypes of PWSI rats with the excitability of dBNST Drd2$^+$ neurons. First, we labeled Drd2$^+$ neurons by injecting Cre-dependent AAV-DIO-EYFP into the dBNST of PWSI rats at day P42. Two weeks later, we performed the EPM, SPT, and FST tests to assess the behavioral performance of each PWSI subject, one test for each day. After the behavioral tests, we performed *in vitro* whole-cell patch-clamp recording on brain slices of each PWSI subject to measure the excitability of dBNST Drd2$^+$ neurons (Figures 4A and 4B).

We first analyzed the linear correlation between neuronal excitability of dBNST Drd2$^+$ neurons of PWSI rats and its EPM score (time spent in open arms). The results show that there is a negative correlation between these two factors, although the result was not significant (Figure S10, $p = 0.16$). We speculate that this insignificance is caused by the individual variations of experimental animals, so we categorized the animals into three groups based on their performance in each test. First, for 11 rats tested in the EPM, we defined subjects corresponding to the top three and the bottom three scores as the "more time spent in open arms" and "less time spent in open arms" groups, respectively. We also defined subjects with the top three scores and the bottom three scores as the "longer swim distance" and "shorter swim distance" groups in the FST, respectively. Similarly, we defined subjects with the top three scores and the bottom three scores in the SPT as the "high social preference" and "low social preference" groups, respectively. Our results showed that rats in the "less time spent in open arms" group displayed a higher level of Drd2$^+$ neuron excitability. Specifically, we found that the current injection-induced action potential numbers of this group were higher compared with the "more time spent in open arms" group (Figures 4C and 4D). However, we did not find a correlation between social preference and swim distance with the level of excitability of dBNST Drd2$^+$ neurons in the SPT or FST (Figures 4E–4H). Consistent with PWSI rats, GH rats also displayed a positive correlation between the excitability of dBNST Drd2$^+$ neurons and animals' behavioral scores in the EPM (Figures 4I–4N). These results indicate that the excitability of dBNST Drd2$^+$ neurons is specifically positively correlated with the anxiety-like phenotypes in both PWSI and GH rats.

Moreover, to investigate the association of these three phenotypes in PWSI male rats, we plotted the linear correlations between the EPM and FST score, EPM and SPT score, and SPT and FST score. Notably, the results showed that these three scores in PWSI rats did not display any significant linear correlation (Figures S11A–S11C). Taken together, the above results indicate that the level of anxiety-like phenotypes, but not social preference or passive coping phenotypes, of PWSI rats was specifically positively correlated with the degree of hyperactivation of dBNST Drd2$^+$ neurons.

Chemogenetic activation of dBNST Drd2$^+$ neurons is sufficient to induce anxiety-like behavior

Given that the excitability of dBNST Drd2$^+$ neurons is positively correlated with the anxiety-like phenotype of PWSI male rats, we tested whether manipulation of the activity of dBNST Drd2$^+$ neurons can regulate the anxiety-like phenotype of rats. Toward this aim, at day P42, GH Drd2::Cre transgenic male rats were injected with Cre-dependent AAV-DIO-hM3D or AAV-DIO-mCherry viruses into the dBNST, and behavioral tests were performed after day P56 (Figures 5A and 5B). First, we verified the

Figure 3. Distinct influence of PWSI stress on synaptic transmission of Drd1$^+$ and Drd2$^+$ neurons in dBNST

(A) Examples of mEPSC signals of dBNST Drd1$^+$ neurons in rats from GH and PWSI groups.

(B) Cumulative frequency curves of inter-event interval of mEPSC signals of dBNST Drd1$^+$ neurons from GH and PWSI rats.

(C and D) Comparison of mEPSC frequency and amplitude of dBNST Drd1$^+$ neurons from GH and PWSI groups (Mann-Whitney *U* test, $p = 0.5722$ and $p = 0.1179$, respectively).

(E) Examples of mIPSC signals of dBNST Drd1$^+$ neurons in rats from GH and PWSI groups.

(F) Cumulative frequency curves of inter-event interval of mIPSC signals of dBNST Drd1$^+$ neurons from GH and PWSI rats.

(G and H) Comparison of mIPSC frequency and amplitude of dBNST Drd1$^+$ neurons from GH and PWSI groups (Student's t test, $p = 0.083$ and $p = 0.9605$, respectively).

(I) Examples of mEPSC signals of dBNST Drd2$^+$ neurons of rats from GH and PWSI groups.

(J) Cumulative frequency curves of inter-event interval of mEPSC signal of dBNST Drd2$^+$ neurons from GH and PWSI rats.

(K and L) Comparison of mEPSC frequency and amplitude of dBNST Drd2$^+$ neurons of rats from GH and PWSI groups (Student's t test; K: $p = 0.0249$; L: $p = 0.4391$).

(M) Examples of mIPSC signals of dBNST Drd2$^+$ neurons of rats from GH and PWSI groups.

(N) Cumulative frequency curves of inter-event interval of mIPSC signal of dBNST Drd2$^+$ neurons from GH and PWSI rats.

(O and P) Comparison of mIPSC frequency and amplitude of dBNST Drd2$^+$ neurons of rats from GH and PWSI groups (O: Mann-Whitney *U* test, $p = 0.0031$; P: Student's t test, $p = 0.9112$).

(Q) Schematic of virus injection.

(R) The leftmost panel shows the infection of Drd1$^+$ neurons by AAV-FLEX-mCherry-2A-TVA-2A-RvG virus; the right three panels show retrogradely labeled GFP$^+$ neurons in the dBNST, CeA, and AHC; scale bar, 100 μm.

(S) The leftmost panel shows the infection of Drd2$^+$ neurons by AAV-FLEX-mCherry-2A-TVA-2A-RvG virus; the right four panels show retrogradely labeled GFP$^+$ neurons in dBNST, CeA, and AHC; scale bar, 100 μm. CeM, medial CeA; CeL, lateral CeA; CeC, capsular CeA; BLA, basolateral amygdala; st, stria terminalis; opt, optic tract; AHC, anterior hypothalamic central area.

(T) Comparison of numbers of input neuron to dBNST Drd1$^+$ and Drd2$^+$ neurons (starter cells) from oval BNST and ad-BNST, AHC and CeA (inputs). Data are shown as mean ± SEM. *$p < 0.05$, **$p < 0.01$, Student's t test; n.s., not significant.

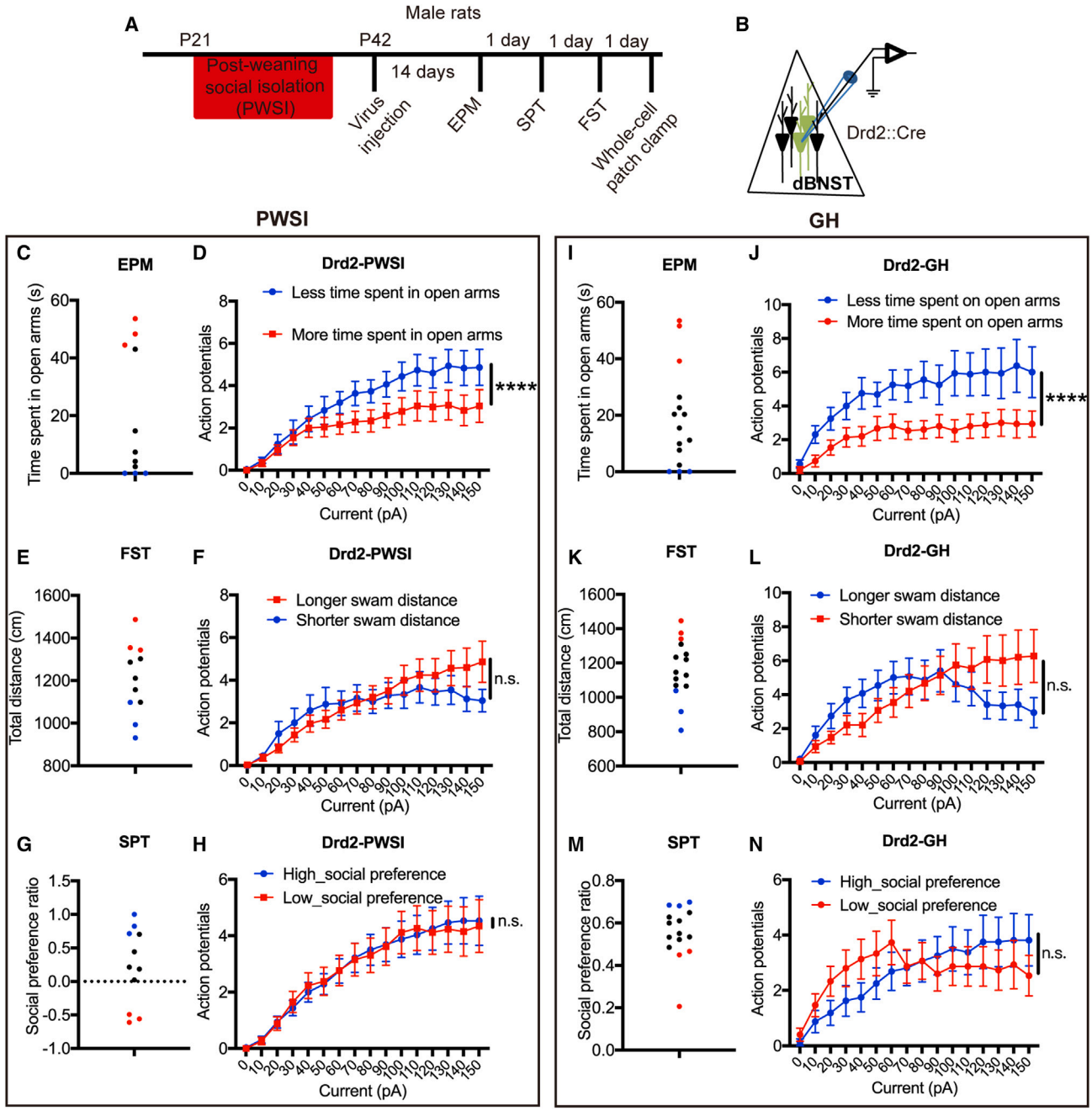

Figure 4. Excitability level of dBNST Drd2$^+$ neurons is positively correlated with its anxiety-like phenotypes in both PWSI and GH male rats

(A) Timeline showing the procedures of PWSI modeling, virus injection, behavioral tests, and whole-cell patch-clamp recording.

(B) Schematic of *in vitro* patch-clamp recording on dBNST Drd2$^+$ neurons labeled by injection of AAV-EF1a-DIO-eYFP.

(C and D) Distribution of the time spent in open arms in the EPM (C) of PWSI rats (n = 11), and step current-induced action potential number (D) of Drd2$^+$ neurons from less time and more time spent in open arms groups (n = 3 for both) of PWSI rats. Red dots represent the three rats that spent the most time in the open arms, while the blue dots represent the three rats that spent the least amount of time in the open arms. Two-way RM ANOVA, open arms avoidance level × step current interaction effects: $F_{15,832} = 0.6614$, p = 0.8235; step current effects: $F_{15,832} = 9.334$, p < 0.0001; open arms avoidance level effects: $F_{1,832} = 27.69$, p < 0.0001.

(E and F) Distribution of the swim distance in the FST (E) of PWSI rats (n = 11), and step current-induced action potential number (F) of Drd2$^+$ neurons from shorter and longer swim distance groups (n = 3 for both) of PWSI rats. Red dots represent the three rats that swam the most, while the blue dots represent the three rats that swam the least. Two-way RM ANOVA, struggling level × step current interaction effects: $F_{15,832} = 0.8235$, p = 0.6518; step current effects: $F_{15,832} = 9.192$, p < 0.0001; struggling level effects: $F_{1,832} = 1.067$, p = 0.3020.

(G and H) Distribution of social preference ratio in SPT (G) of PWSI rats (n = 11) and step current-induced action potential number (H) of Drd2$^+$ neurons from high and low social preference groups (n = 3 for both) of PWSI rats. Red dots represent the three rats that had the highest social preference ratio, while the blue dots

(legend continued on next page)

expression specificity of the AAV-DIO-hM3D virus and confirmed by *ex vivo* brain slice recording that application of clozapine-N-oxide (CNO) was sufficient to activate the corresponding neurons (Figures 5C and 5D). Then we performed the behavioral tests. We found that rats in the hM3D-expressing group showed less time spent in the open arms in EPM, but no significant change was noted in open arm entry number or total moving distance (Figures 5E and 5F) after CNO treatment compared with the mCherry-expressing group. Consistent with the EPM results, we also found that the hM3D-expressing group spent less time in the center and had fewer center entries in the OFT but did not display a difference in the total distance that rats moved (Figures 5G and 5H). Taken together, these results indicate that activation of dBNST Drd2$^+$ neurons could specifically induce anxiety-like behavior. However, we did not observe a significant effect of activation of Drd2$^+$ neurons on passive coping behavior or social preference, as indicated by the results of the FST and SPT (Figures S12A and S12B). Consistent with the results for male rats, we found that activation of dBNST Drd2$^+$ neurons also has the tendency to increase the anxiety-like behavior in female rats (Figures S13A and S13B).

Hyperfunction of dBNST Drd2 receptors displays an anxiolytic effect

The Drd2 receptor is a G protein-coupled, inwardly rectifying potassium channel,[28] activation of which hyperpolarizes neurons. Thus, we examined whether application of a Drd2 agonist in the dBNST could hyperpolarize the Drd2$^+$ neurons therein and result in an anxiolytic effect. We first labeled the dBNST Drd2$^+$ neurons by injection of AAV-DIO-EYFP into the dBNST of Drd2::Cre rats and confirmed the effect of a Drd2 agonist, quinpirole, on dBNST Drd2$^+$ neurons at the cellular level by patch-clamp recording (Figure 6A). As expected, we found that local application of quinpirole in dBNST indeed hyperpolarized Drd2$^+$ neurons (Figure 6B). Then, we examined the effect of quinpirole to dBNST on the behavior of GH rats (Figure 6C). Our results showed that intra-dBNST infusion of quinpirole increased the time that GH rats spent in the open arms compared with saline-treated rats but did not affect the total distance that rats moved in the EPM (Figures 6D–6F and S14A). Consistently, we also found that the quinpirole-treated group showed increased time in the center compared with the saline-treated group in the OFT (Figures 6G and 6H). These results indicated that activation of the Drd2 receptor decreased the excitability of Drd2$^+$ neurons and induced an anxiolytic effect, further supporting the findings from neuronal manipulation. However, in the SPT, the social preference ratio was comparable between quinpirole- and saline-treated groups (Figure S14B).

The above results suggest that Drd2 signaling in dBNST neurons has anxiolytic effects. Then, we examined the modulation effects of Drd2 signaling on neuronal excitability between GH and PWSI rats. We first labeled the dBNST Drd2$^+$ neurons by injection of AAV-DIO-EYFP into the dBNST of Drd2::Cre rats and performed patch-clamp recording (Figure 6I). The results showed that the number of action potentials of dBNST Drd2$^+$ neurons was decreased by quinpirole in both GH and PWSI male rats. However, the negative modulation effects were smaller in the PWSI group (Figure 6J), suggesting that Drd2$^+$ neurons are less sensitive to quinpirole, i.e., there is a functional impairment in dBNST Drd2 receptors in PWSI male rats. Taken together, these results indicate that hyperfunction of Drd2 receptors in the dBNST is sufficient for an anxiolytic effect, implying that the functional impairment of dBNST Drd2 receptors in Drd2$^+$ neurons underlies the PWSI-induced anxiety-like behavior. Interestingly, consistent with the effect of PWSI stress on the behavioral phenotype of female rats, the negative modulation effects of quinpirole on the function of Drd2 receptors of dBNST Drd2$^+$ neurons were comparable in GH and PWSI female rats (Figure 6K).

Chronic inhibition of dBNST Drd2$^+$ neurons ameliorated anxiety-like behaviors of PWSI rats

As described above, we found that dBNST Drd2$^+$ neurons were hyperactive in PWSI rats (Figure 2), and activation of Drd2$^+$ neurons was sufficient to induce anxiety-like behavior (Figure 5). We then tested whether the PWSI-induced anxiety-like behavioral phenotype could be reversed through manipulation of the activity of dBNST Drd2$^+$ neurons. We found that overexpression of an inward rectifying potassium channel (Kir4.1), which hyperpolarizes and inactivates cells, indeed hyperpolarized dBNST Drd2$^+$ neurons (Figures 7A–7D). Furthermore, chronic inhibition of Drd2$^+$ neurons by overexpression of Kir4.1 increased the time that PWSI rats spent in the open arms and the number of open arms entries but had no significant effect on the total distance that rats moved in the EPM (Figures 7E and 7F). The results of the OFT test also showed that chronic inhibition of Drd2$^+$ neurons in PWSI rats could increase the time that rats spent in the center, number of center entries, and total distance traveled (Figures 7G and 7H). We also found that chronic inhibition of dBNST Drd2$^+$ neurons in PWSI rats increased the time that rats spent in the light box and the number of light box entries in the L-D box test

represent rats with the lowest social preference ratio. Two-way RM ANOVA, social preference level × step current interaction effects: $F_{15,896} = 0.04977$, $p > 0.9999$; step current effects: $F_{15,896} = 12.86$, $p < 0.0001$; social preference level effects: $F_{1,896} = 0.01057$, $p = 0.9181$.

(I and J) Distribution of the time spent in open arms in the EPM (I) of GH rats (n = 15) and step current-induced action potential number (J) of Drd2$^+$ neurons from less time and more time spent in open arms groups (n = 3 for both) of GH rats. Two-way RM ANOVA, open arms avoidance level × step current interaction effects: $F_{15,464} = 0.3955$, $p = 0.9801$; step current effects: $F_{15,464} = 3.429$, $p < 0.0001$; open arms avoidance level effects: $F_{1,464} = 59.26$, $p < 0.0001$.

(K and L) Distribution of the swim distance in FST (K) of GH rats (n = 15) and step current-induced action potential number (L) of Drd2$^+$ neurons from shorter and longer swim distance groups (n = 3 for both) of GH rats. Two-way RM ANOVA, struggling level × step current interaction effects: $F_{15,448} = 1.662$, $p = 0.0554$; step current effects: $F_{15,448} = 4.789$, $p < 0.0001$; struggling level effects: $F_{1,448} = 0.5582$, $p = 0.4554$.

(M and N) Distribution of social preference ratio in SPT (M) of GH rats (n = 15) and step current-induced action potential number (N) of Drd2$^+$ neurons from high and low social preference groups (n = 3 for both) of GH rats. Two-way RM ANOVA, social preference level × step current interaction effects: $F_{15,464} = 0.8736$, $p = 0.5944$; step current effects: $F_{15,464} = 3.231$, $p < 0.0001$; social preference level effects: $F_{1,464} = 0.05381$, $p = 0.8167$. Data are shown as mean ± SEM; ****$p < 0.0001$; n.s., not significant.

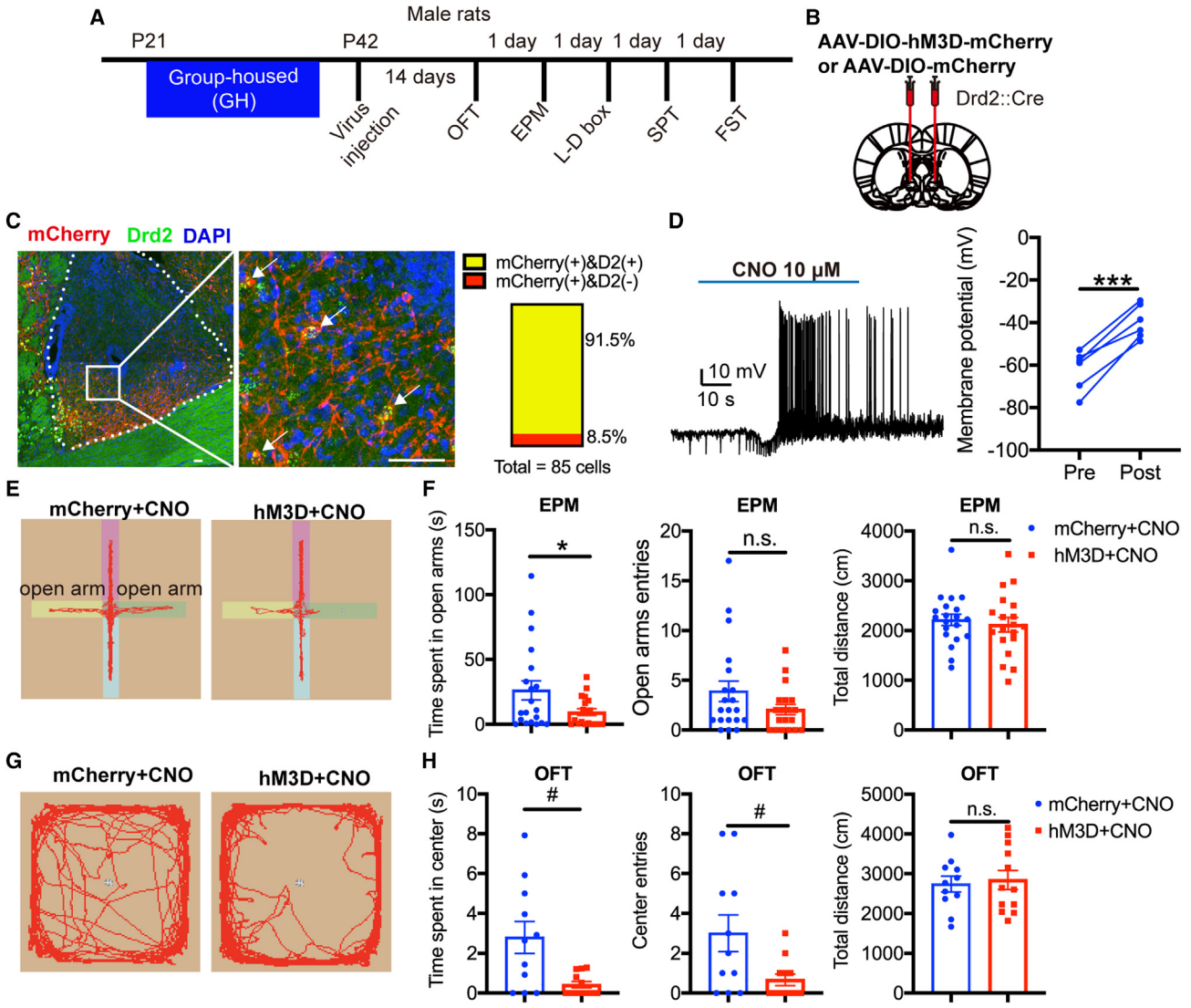

Figure 5. Chemogenetic activation of dBNST Drd2$^+$ neurons are sufficient to induce anxiety-like behavior

(A) Timeline shows the procedures of virus injection and behavioral tests.

(B) Schematic of bilateral injection of virus into dBNST of Drd2::Cre rats.

(C) Left is the expression pattern of AAV-hSyn-DIO-hM3D-mCherry in Drd2$^+$ neurons in the dBNST of Drd2::Cre rats; red represents the AAV-hSyn-DIO-hM3D-mCherry, green represents Drd2 mRNA, and blue represents nuclei stained with DAPI; scale bar represents 50 μm. The windowed area is enlarged; white arrows indicate the mCherry and Drd2 mRNA colabeled neurons. The right panel shows the statistics of the co-labeling rate of mCherry and Drd2 mRNA.

(D) Left is an example of the CNO-induced neuronal response of hM3D-expressing neurons in the dBNST *in vitro*. Right is the comparison of membrane potentials of hM3D-expressing neurons before and after CNO delivery (paired Student's t test, p = 0.0003).

(E) Examples of locomotion trajectory of mCherry-expressing and hM3D-expressing rats in EPM after intraperitoneal (i.p.) injection of CNO.

(F) Statistics of results from EPM test of mCherry-expressing and hM3D-expressing rats after i.p. injection of CNO. The left, middle, and right panels respectively show the time rats spent in open arms, the number of open arm entries, the total distance moved in EPM test (Student's t test, left, p = 0.0432; middle, p = 0.1226; right, p = 0.6195).

(G) Examples of locomotion trajectory of mCherry-expressing and hM3D-expressing rats in OFT after i.p. injection of CNO.

(H) Statistics of results from OFT of mCherry-expressing and hM3D-expressing rats after i.p. injection of CNO. The left, middle, and right panels, respectively, show the time the rat spent in the center, the number of center entries, and the total distance that rats moved in the OFT (Mann-Whitney *U* test, p = 0.0149; Mann-Whitney *U* test, p = 0.0432; Student's t test, t = 0.344, p = 0.7343). Data are shown as mean ± SEM; *p < 0.05, ***p < 0.001, ****p < 0.0001, Student's t test; n.s., not significant; #p < 0.05, Mann-Whitney *U* test.

(Figures 7I and 7J). Together, the results of the EPM, OFT, and L-D box demonstrated that chronic inhibition of Drd2$^+$ neurons in the dBNST did ameliorate the PWSI-induced anxiety-like behavior. However, we did not observe any significant difference between Kir4.1- and eGFP-expressing PWSI rats in the FST and SPT (Figures 7K and 7L).

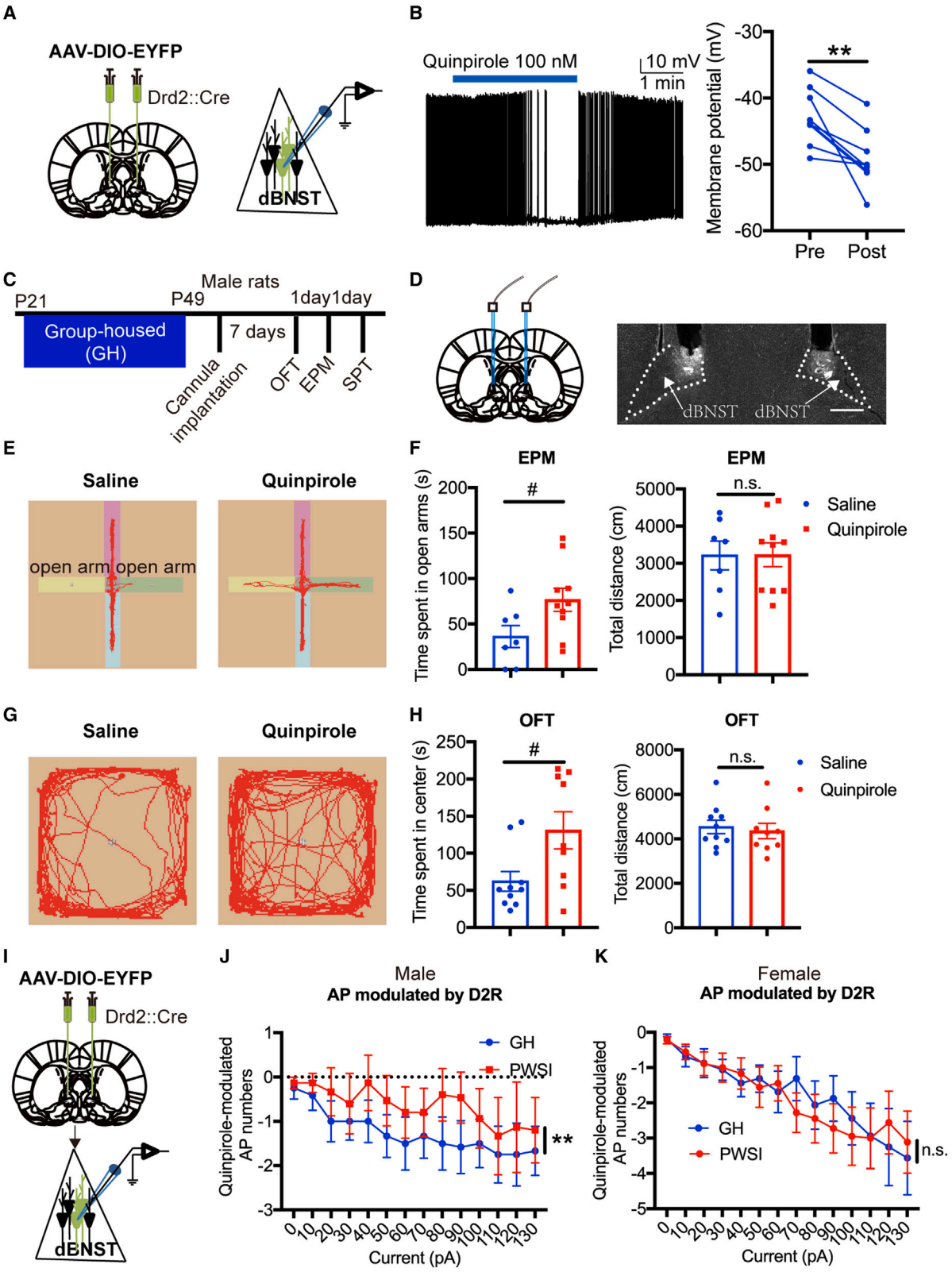

(legend on next page)

DISCUSSION

We found that the excitability of dBNST Drd2$^+$ neurons displayed a sex-specific increase and was positively correlated with the level of anxiety-like behavior of PWSI male rats. The sufficiency and necessity of these neurons in mediating PWSI-induced anxiety-like behaviors in male rats were demonstrated by the results of activation and chronic inhibition of Drd2$^+$ neurons. The results of our pharmacological studies indicate that the dysfunction of Drd2 receptors of Drd2$^+$ neurons underlies the hyperactivation of Drd2$^+$ neurons in the dBNST of PWSI male rats. Our findings suggest that dBNST Drd2$^+$ neurons are a potential target for therapeutic intervention to treat social isolation-induced disorders.

Social stimuli are considered a factor that plays a key role in the maintenance of homeostasis, and a long-lasting deteriorating social environment could impair the homeostatic regulation of a social network.[29,30] The adolescent period is sensitive to external stressors, and our PWSI model—with the time window of P21 to P56—coincides with the adolescent period of rodents.[31] Anxiety-like behavior and social withdrawal phenotypes were clearly observed in our experiments (Figure 1). The sex-specific influence of PWSI stress on the anxiety-like behavior and stressful state present in our results was consistent with previous work,[32] which found that male, but not female, rats displayed anxiety-like behavior after PWSI. Notably, inconsistent with some previous studies,[33,34] we did not observe the hyperlocomotion of PWSI rats. On the contrary, the locomotion of PWSI male rats exhibited a decrease in the OFT (Figure 1E), which may have resulted from the different protocols of social isolation procedures. Consistent with the results of Kinley et al.,[35] we also found that the sociality of PWSI male rats decreased (Figures 1H and 1I). However, decrease of sociality was also observed in female mice by other groups.[36,37] We speculated this inconsistency may attribute to the difference of species. In contrast to the results of previous studies,[38,39] we did not find that social isolation in adulthood (P56-P91) had significant influence on the anxiety-like behaviors (Figure S2). We speculate that this is possibly caused by the difference of durations of social isolation manipulation and rearing conditions.

DA systems, which are highly involved in the regulation of reward and motivation,[40–42] display dysfunction in chronic stress-related animal models—including chronic social isolation.[6,15] However, the relationship between the dysfunction of DA systems and social isolation-induced behavioral deficits, especially emotional disorders, remains unclear. In the present study, we found that a major type of DA receptor—Drd2—showed functional impairment (Figure 6J), potentially underlying the hyperactivity of dBNST Drd2$^+$ neurons (Figure 2). In fact, previous studies found that social isolation had no effect on the expression or activity of Drd2 receptors in the nucleus accumbens, prefrontal cortex, hippocampus, or amygdala of male rats.[43] Thus, the Drd2 receptors in the dBNST may be a specific target for DA systems to play their role in regulating social isolation-induced emotional disorders. Notably, since Drd2 receptors show a higher affinity than Drd1 receptors for dopamine in the brain,[44] the dopamine level in the dBNST is highly likely to be significantly influenced by the PWSI stress. However, since we could not exclude the function of presynaptic Drd2 receptors in dBNST, the role of dBNST presynaptic Drd2 receptors in PWSI-induced anxiety-like behavior remain to be fully understood.

The results of mEPSC and mIPSC recording of Drd1$^+$ and Drd2$^+$ neurons indicate that the net excitatory input of dBNST Drd2$^+$, but not Drd1$^+$, neurons of PWSI male rats is specifically increased (Figure 3). As a result, the increased excitability combined with increased net excitatory input exacerbated the hyperactivity of Drd2$^+$ neurons in PWSI male rats. Furthermore, the specific increase of net excitatory input may result from the specific plasticity change of the afferents of dBNST Drd2$^+$, but not Drd1$^+$, neurons, implying that the specific afferents of Drd2$^+$ neurons of the dBNST may also serve as a potential target to alleviate the anxiety-like behaviors induced by PWSI stress.

Figure 6. Sex-specific correlation of functional impairment of dBNST D2 receptor to PWSI-induced anxiety-like behavior

(A) Left panel: schematic of bilateral injection of AAV-EF1a-DIO-eYFP into the dBNST of Drd2::Cre rats; right panel: schematic of *in vitro* recording of EYFP$^+$ neurons.

(B) Application of quinpirole decreased the excitability of Drd2$^+$ neurons *in vitro*. The left panel shows examples of inhibitory responses of Drd2$^+$ neurons to quinpirole, and the right panel shows the comparison of membrane potentials of Drd2$^+$ neurons before and after quinpirole delivery (paired Student's t test, p = 0.0022).

(C) Timeline shows the procedures of cannula implantation and behavioral tests.

(D) Left panel: schematic of cannula implantation; right panel: example of cannula implantation locus; scale bar represents 500 μm.

(E) Example of locomotion trajectory of rats from saline- and quinpirole-treated GH rats in the EPM.

(F) Comparison of the time spent in the open arms and total distance moved in the EPM by saline- and quinpirole-treated GH rats (Mann-Whitney *U* test, p = 0.0417; for total distance: Mann-Whitney *U* test, p = 0.8683).

(G) Example of locomotion trajectory of saline- and quinpirole-treated GH rats in the OFT.

(H) Comparison of time spent in the center and total distance traveled in the OFT by saline- and quinpirole-treated GH rats (Mann-Whitney *U* test, p = 0.0331; for total distance: Student's t test, p = 0.6906).

(I) Top panel: schematic of bilateral injection of AAV-EF1a-DIO-eYFP into dBNST of Drd2Cre rats; bottom panel: schematic of *in vitro* recording of EYFP$^+$ neurons.

(J) Comparison of the decrease in current injection-induced action potentials of dBNST Drd2$^+$ neurons from GH and PWSI male rats after quinpirole administration (two-way RM ANOVA, housing [GH vs. PWSI] × step current interaction effects: $F_{13,350} = 0.1131$, p > 0.9999; step current effects: $F_{13,350} = 0.9467$, p = 0.5045; housing [GH vs. PWSI] effects: $F_{1,350} = 7.353$, p = 0.007).

(K) Comparison of the decrease in current injection-induced action potentials of dBNST Drd2$^+$ neurons from GH and PWSI female rats after quinpirole administration (two-way RM ANOVA, housing [GH vs. PWSI] × step current interaction effects: $F_{13,448} = 0.2714$, p = 0.9951; step current effects: $F_{13,448} = 4.564$, p < 0.0001; housing [GH vs. PWSI] effects: $F_{1,448} = 1275$, p = 0.7212). Data are shown as mean ± SEM; **p < 0.01, Student's t test; n.s., not significant; #p < 0.05, Mann-Whitney *U* test.

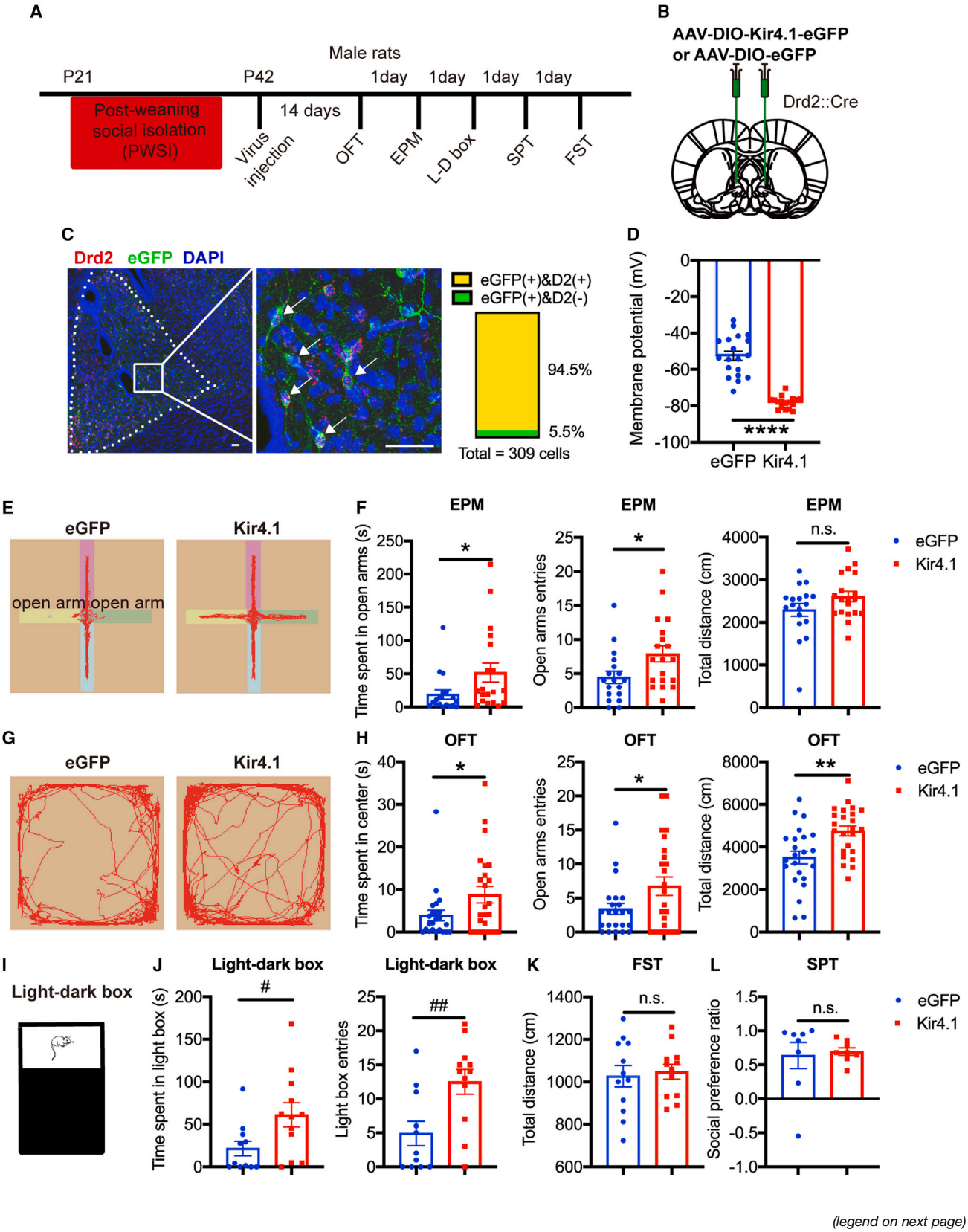

(legend on next page)

Previous studies have found that there are significant differences between males and females in the neuroanatomy and release properties of dopamine systems. These sex-specific differences may mediate the distinct susceptibility of males and females to mental illness.[45–47] Moreover, BNST, which is a sexually dimorphic nucleus[48,49] and a pivotal nucleus that regulates the stress response,[16] also expresses DA receptors.[27] Indeed, the results of our work demonstrate that the different influence of PWSI stress on the excitability of dBNST Drd2$^+$ neurons in male and female rats underlies the sex-specific anxiety-like phenotype (Figures 2 and 7). Furthermore, this is likely mediated by the functional change in dBNST Drd2 receptors (Figure 6). These functional changes may include that the expression level or the sensitivity of dBNST Drd2 receptor was decreased in PWSI male rats, or the dynamics of dBNST dopamine turnover have sex-differences and which in turn results in sex-specific influence of PWSI stress on male and female Drd2$^+$ neurons. These plausible mechanisms remain to be well studied.

PWSI is a chronic modeling protocol,[50] so changes in neuronal plasticity in the dBNST may also be a chronic process. We found that chemogenetic activation of dBNST Drd2$^+$ neurons in GH rats only partially recapitulated the anxiety-like behaviors observed in PWSI rats in the OFT and EPM (Figures 5F and 5H vs. 1C and 1E). We speculate that this is likely due to the inability of the CNO-mediated chemogenetic activation in our protocol to fully reproduce the chronic stress of PWSI. For this reason, chronic inhibition of dBNST Drd2$^+$ neurons in PWSI rats showed significant alleviation of anxiety-like behaviors in all three tests of anxiety-like behavior (Figure 7). Since our results showed that dBNST Drd2$^+$ neurons only mediate the PWSI stress-induced anxiety-like behavior but not social deficits, we speculate that these phenotypes may be mediated by different neuronal populations. Moreover, as the results showed in Figures 1C, 5F, and 7F, the baseline levels of anxiety-like behavior in the EPM test are different. This may be attributed to the different experimental conditions and manipulations on control rats. For instance, the animals in Figure 1C are wild-type rats and did not undergo surgery, while the animals in Figure 5F are surgically operated and injected with virus. The animals in Figure 7F are PWSI-treated, surgically operated, and injected with virus. Taken together, the difference in surgery states and PWSI-treatments might change the baselines of behavioral results.

Limitations of the study

In this study, we used the behavioral tests that merely scored the anxiety-like, depression-like, and social preference level of rats, so we could not exclude whether other functions of animals were impaired by PWSI stress. Moreover, due to the limitation of behavioral tests that we used to evaluate the function of dBNST Drd2$^+$ neurons, functions of this population of neurons may not just mediate the anxiety-like behavior after PWSI stress. Finally, since we did not dissect the plastic change of specific upstream of dBNST Drd2$^+$ neurons, e.g., AHC and CeA, it is of great importance to investigate the role of these inputs in PWSI-induced sex-specific anxiety-like behavior.

STAR★METHODS

Detailed methods are provided in the online version of this paper and include the following:

- KEY RESOURCES TABLE
- RESOURCE AVAILABILITY
  - Lead contact
  - Materials availability
  - Data and code availability
- EXPERIMENTAL MODEL AND SUBJECT DETAILS
- METHOD DETAILS
  - PWSI modeling procedure
  - Behavioral tests
  - Open field test (OFT)
  - Elevated plus maze (EPM) test
  - Light-dark box test (L-D box)
  - Forced swim test (FST)
  - Three-chamber social preference test (SPT)
  - Measurement of corticosterone
  - Electrophysiology
  - Viruses
  - Stereotaxic surgery and microinjection
  - Immunohistology and imaging

Figure 7. Chronic inhibition of Drd2$^+$ neurons in the dBNST of PWSI male rats ameliorated PWSI-induced anxiety-like behaviors

(A) Timeline shows the procedures of PWSI modeling, virus injection, and behavioral tests.

(B) Schematic of bilateral injection of virus into dBNST of Drd2::Cre rats.

(C) Left is the expression pattern of AAV-EF1a-DIO-Kir4.1-eGFP in Drd2$^+$ neurons in the dBNST of Drd2::Cre rats; green represents AAV-EF1a-DIO-Kir4.1-eGFP, red represents Drd2 mRNA, and blue represents nuclei stained with DAPI. The windowed area is enlarged, and white arrows indicate the eGFP and Drd2 mRNA colabeled neurons; scale bar represents 50 μm; right panel shows the colabel rate of eGFP and Drd2 mRNA.

(D) Comparison of membrane potential of eGFP- and Kir4.1-expressing Drd2$^+$ neurons in the dBNST of GH rats (Student's t test, $p < 0.0001$).

(E) Example of locomotion trajectory of eGFP- and Kir4.1-expressing PWSI rats in EPM.

(F) Statistic of results from EPM of eGFP- and Kir4.1-expressing PWSI rats; left panel shows the time rats spent in open arms, middle panel shows the number of open arm entries, and right panel shows the total distance traveled (Mann-Whitney *U* test, $p = 0.0184$, 0.0262, 0.21 for corresponding test).

(G) Example of locomotion trajectory of eGFP- and Kir4.1-expressing PWSI rats in OFT.

(H) Statistics from OFT of eGFP- and Kir4.1-expressing PWSI rats; left panel shows the time rats spent in center, middle panel shows the number of center entries, and right panel shows the total distance traveled (Student's t test, left, $p = 0.0425$, middle, $p = 0.0414$, right, $p = 0.002$).

(I) Schematic of L-D box test.

(J) Comparison of the time rats spent in light box and number of light box entries by eGFP- and Kir4.1-expressing PWSI rats (Mann-Whitney *U* test, $p = 0.0125$, 0.0088 for corresponding tests).

(K) Comparison of total swimming distance of eGFP-expressing and Kir4.1-expressing rats in the FST (Student's t test, $p = 0.7413$).

(L) Comparison of social preference ratio of eGFP- and Kir4.1-expressing rats in the SPT (Mann-Whitney *U* test, $p = 0.2345$). Data are shown as mean ± SEM; *$p < 0.05$, Student's t test; n.s., not significant; #$p < 0.05$, ##$p < 0.01$, Mann-Whitney *U* test.

SUPPLEMENTAL INFORMATION

Supplemental information can be found online at https://doi.org/10.1016/j.celrep.2023.112799.

ACKNOWLEDGMENTS

We would like to thank Dr. Wen Zhang for electrophysiological data analysis and Liu Fan for the patch-clamp recording instructions. We are also grateful to technical support from the optical imaging facility and animal facility of the Institute of Neuroscience, Center for Brain Science and Intelligence Technology, CAS.

This work was supported in part by the STI2030-Major Projects (2022ZD0205100), Strategic Priority Research Program of the Chinese Academy of Science (Grant No. XDB32010300), and Shanghai Municipal Science and Technology Major Project (Grant No. 2018SHZDZX05) to Z.W., and CAMS Innovation Fund for Medical Sciences (2019-I2M-5-014) to H.G.

AUTHOR CONTRIBUTIONS

C.Z. and Z.W. designed the experiments and wrote the paper. L.W. and C.Z. performed the electrophysiological recording and analysis. C.Z., L.W., B.L., and S.W. performed the behavioral tests, immunofluorescence staining, and analysis. Q.W. and Y.H. bred and genotyped all rats. X.L. and H.G. contributed to the *trans*-synaptic labeling experiments.

DECLARATION OF INTERESTS

The authors declare no competing interests.

Received: September 4, 2022
Revised: May 7, 2023
Accepted: June 26, 2023
Published: July 14, 2023

REFERENCES

1. Einon, D.F., and Morgan, M.J. (1977). A critical period for social isolation in the rat. Dev. Psychobiol. *10*, 123–132.
2. Bicks, L.K., Yamamuro, K., Flanigan, M.E., Kim, J.M., Kato, D., Lucas, E.K., Koike, H., Peng, M.S., Brady, D.M., Chandrasekaran, S., et al. (2020). Prefrontal parvalbumin interneurons require juvenile social experience to establish adult social behavior. Nat. Commun. *11*, 1003.
3. Makinodan, M., Rosen, K.M., Ito, S., and Corfas, G. (2012). A critical period for social experience-dependent oligodendrocyte maturation and myelination. Science *337*, 1357–1360.
4. Lin, S., Li, X., Chen, Y.H., Gao, F., Chen, H., Hu, N.Y., Huang, L., Luo, Z.Y., Liu, J.H., You, Q.L., et al. (2018). Social Isolation During Adolescence Induces Anxiety Behaviors and Enhances Firing Activity in BLA Pyramidal Neurons via mGluR5 Upregulation. Mol. Neurobiol. *55*, 5310–5320.
5. Yamamuro, K., Bicks, L.K., Leventhal, M.B., Kato, D., Im, S., Flanigan, M.E., Garkun, Y., Norman, K.J., Caro, K., Sadahiro, M., et al. (2020). A prefrontal-paraventricular thalamus circuit requires juvenile social experience to regulate adult sociability in mice. Nat. Neurosci. *23*, 1240–1252.
6. King, M.V., Seeman, P., Marsden, C.A., and Fone, K.C.F. (2009). Increased dopamine D2High receptors in rats reared in social isolation. Synapse *63*, 476–483.
7. Heidbreder, C.A., Weiss, I.C., Domeney, A.M., Pryce, C., Homberg, J., Hedou, G., Feldon, J., Moran, M.C., and Nelson, P. (2000). Behavioral, neurochemical and endocrinological characterization of the early social isolation syndrome. Neuroscience *100*, 749–768.
8. Dalley, J.W., Theobald, D.E., Pereira, E.A.C., Li, P.M.M.C., and Robbins, T.W. (2002). Specific abnormalities in serotonin release in the prefrontal cortex of isolation-reared rats measured during behavioural performance of a task assessing visuospatial attention and impulsivity. Psychopharmacology (Berl) *164*, 329–340.
9. Park, G., Ryu, C., Kim, S., Jeong, S.J., Koo, J.W., Lee, Y.S., and Kim, S.J. (2021). Social isolation impairs the prefrontal-nucleus accumbens circuit subserving social recognition in mice. Cell Rep. *35*, 109104.
10. Lukkes, J.L., Watt, M.J., Lowry, C.A., and Forster, G.L. (2009). Consequences of post-weaning social isolation on anxiety behavior and related neural circuits in rodents. Front. Behav. Neurosci. *3*, 18.
11. Grace, A.A. (2016). Dysregulation of the dopamine system in the pathophysiology of schizophrenia and depression. Nat. Rev. Neurosci. *17*, 524–532.
12. Hung, L.W., Neuner, S., Polepalli, J.S., Beier, K.T., Wright, M., Walsh, J.J., Lewis, E.M., Luo, L., Deisseroth, K., Dölen, G., and Malenka, R.C. (2017). Gating of social reward by oxytocin in the ventral tegmental area. Science *357*, 1406–1411.
13. Whitaker, L.R., Degoulet, M., and Morikawa, H. (2013). Social deprivation enhances VTA synaptic plasticity and drug-induced contextual learning. Neuron *77*, 335–345.
14. Fulford, A.J., and Marsden, C.A. (2007). An intact dopaminergic system is required for context-conditioned release of 5-HT in the nucleus accumbens of postweaning isolation-reared rats. Neuroscience *149*, 392–400.
15. Brenes, J.C., and Fornaguera, J. (2009). The effect of chronic fluoxetine on social isolation-induced changes on sucrose consumption, immobility behavior, and on serotonin and dopamine function in hippocampus and ventral striatum. Behav. Brain Res. *198*, 199–205.
16. Daniel, S.E., and Rainnie, D.G. (2016). Stress Modulation of Opposing Circuits in the Bed Nucleus of the Stria Terminalis. Neuropsychopharmacology *41*, 103–125.
17. Davis, M., Walker, D.L., Miles, L., and Grillon, C. (2010). Phasic vs sustained fear in rats and humans: role of the extended amygdala in fear vs anxiety. Neuropsychopharmacology *35*, 105–135.
18. Dong, H.W., and Swanson, L.W. (2004). Organization of axonal projections from the anterolateral area of the bed nuclei of the stria terminalis. J. Comp. Neurol. *468*, 277–298.
19. Dong, H.W., Petrovich, G.D., Watts, A.G., and Swanson, L.W. (2001). Basic organization of projections from the oval and fusiform nuclei of the bed nuclei of the stria terminalis in adult rat brain. J. Comp. Neurol. *436*, 430–455.
20. Rodriguez-Romaguera, J., Ung, R.L., Nomura, H., Otis, J.M., Basiri, M.L., Namboodiri, V.M.K., Zhu, X., Robinson, J.E., van den Munkhof, H.E., McHenry, J.A., et al. (2020). Prepronociceptin-Expressing Neurons in the Extended Amygdala Encode and Promote Rapid Arousal Responses to Motivationally Salient Stimuli. Cell Rep. *33*, 108362.
21. Zelikowsky, M., Hui, M., Karigo, T., Choe, A., Yang, B., Blanco, M.R., Beadle, K., Gradinaru, V., Deverman, B.E., and Anderson, D.J. (2018). The Neuropeptide Tac2 Controls a Distributed Brain State Induced by Chronic Social Isolation Stress. Cell *173*, 1265–1279.e19.
22. Hu, P., Liu, J., Maita, I., Kwok, C., Gu, E., Gergues, M.M., Kelada, F., Phan, M., Zhou, J.N., Swaab, D.F., et al. (2020). Chronic Stress Induces Maladaptive Behaviors by Activating Corticotropin-Releasing Hormone Signaling in the Mouse Oval Bed Nucleus of the Stria Terminalis. J. Neurosci. *40*, 2519–2537.
23. Hasue, R.H., and Shammah-Lagnado, S.J. (2002). Origin of the dopaminergic innervation of the central extended amygdala and accumbens shell: a combined retrograde tracing and immunohistochemical study in the rat. J. Comp. Neurol. *454*, 15–33.
24. Yu, W., Pati, D., Pina, M.M., Schmidt, K.T., Boyt, K.M., Hunker, A.C., Zweifel, L.S., McElligott, Z.A., and Kash, T.L. (2021). Periaqueductal

gray/dorsal raphe dopamine neurons contribute to sex differences in pain-related behaviors. Neuron *109*, 1365–1380.e5.

25. Sim, H.R., Choi, T.Y., Lee, H.J., Kang, E.Y., Yoon, S., Han, P.L., Choi, S.Y., and Baik, J.H. (2013). Role of dopamine D2 receptors in plasticity of stress-induced addictive behaviours. Nat. Commun. *4*, 1579.
26. Tadori, Y., Forbes, R.A., McQuade, R.D., and Kikuchi, T. (2008). Characterization of aripiprazole partial agonist activity at human dopamine D3 receptors. Eur. J. Pharmacol. *597*, 27–33.
27. Kim, S.Y., Adhikari, A., Lee, S.Y., Marshel, J.H., Kim, C.K., Mallory, C.S., Lo, M., Pak, S., Mattis, J., Lim, B.K., et al. (2013). Diverging neural pathways assemble a behavioural state from separable features in anxiety. Nature *496*, 219–223.
28. Michaeli, A., and Yaka, R. (2010). Dopamine inhibits GABA(A) currents in ventral tegmental area dopamine neurons via activation of presynaptic G-protein coupled inwardly-rectifying potassium channels. Neuroscience *165*, 1159–1169.
29. Matthews, G.A., and Tye, K.M. (2019). Neural mechanisms of social homeostasis. Ann. N. Y. Acad. Sci. *1457*, 5–25.
30. Huang, S.H., Liu, W.Z., Qin, X., Guo, C.Y., Xiong, Q.C., Wang, Y., Hu, P., Pan, B.X., and Zhang, W.H. (2022). Association of Increased Amygdala Activity with Stress-Induced Anxiety but not Social Avoidance Behavior in Mice. Neurosci. Bull. *38*, 16–28.
31. Andersen, S.L. (2003). Trajectories of brain development: point of vulnerability or window of opportunity? Neurosci. Biobehav. Rev. *27*, 3–18.
32. Weiss, I.C., Pryce, C.R., Jongen-Rêlo, A.L., Nanz-Bahr, N.I., and Feldon, J. (2004). Effect of social isolation on stress-related behavioural and neuroendocrine state in the rat. Behav. Brain Res. *152*, 279–295.
33. Einon, D.F., and Morgan, M.J. (1978). Early isolation produces enduring hyperactivity in the rat, but no effect upon spontaneous alternation. Q. J. Exp. Psychol. *30*, 151–156.
34. Gentsch, C., Lichtsteiner, M., Frischknecht, H.R., Feer, H., and Siegfried, B. (1988). Isolation-induced locomotor hyperactivity and hypoalgesia in rats are prevented by handling and reversed by resocialization. Physiol. Behav. *43*, 13–16.
35. Kinley, B.L., Kyne, R.F., Lawton-Stone, T.S., Walker, D.M., and Paul, M.J. (2021). Long-term consequences of peri-adolescent social isolation on social preference, anxiety-like behaviour, and vasopressin neural circuitry of male and female rats. Eur. J. Neurosci. *54*, 7790–7804.
36. Wang, Z.J., Shwani, T., Liu, J., Zhong, P., Yang, F., Schatz, K., Zhang, F., Pralle, A., and Yan, Z. (2022). Molecular and cellular mechanisms for differential effects of chronic social isolation stress in males and females. Mol. Psychiatry *27*, 3056–3068.
37. Tan, T., Wang, W., Liu, T., Zhong, P., Conrow-Graham, M., Tian, X., and Yan, Z. (2021). Neural circuits and activity dynamics underlying sex-specific effects of chronic social isolation stress. Cell Rep. *34*, 108874.
38. Zorzo, C., Méndez-López, M., Méndez, M., and Arias, J.L. (2019). Adult social isolation leads to anxiety and spatial memory impairment: Brain activity pattern of COx and c-Fos. Behav. Brain Res. *365*, 170–177.
39. Ieraci, A., Mallei, A., and Popoli, M. (2016). Social Isolation Stress Induces Anxious-Depressive-Like Behavior and Alterations of Neuroplasticity-Related Genes in Adult Male Mice. Neural Plast. *2016*, 6212983.
40. Eshel, N., Tian, J., Bukwich, M., and Uchida, N. (2016). Dopamine neurons share common response function for reward prediction error. Nat. Neurosci. *19*, 479–486.
41. Yao, Y., Gao, G., Liu, K., Shi, X., Cheng, M., Xiong, Y., and Song, S. (2021). Projections from D2 Neurons in Different Subregions of Nucleus Accumbens Shell to Ventral Pallidum Play Distinct Roles in Reward and Aversion. Neurosci. Bull. *37*, 623–640.
42. Solié, C., Girard, B., Righetti, B., Tapparel, M., and Bellone, C. (2022). VTA dopamine neuron activity encodes social interaction and promotes reinforcement learning through social prediction error. Nat. Neurosci. *25*, 86–97.
43. Walker, D.M., Cunningham, A.M., Gregory, J.K., and Nestler, E.J. (2019). Long-Term Behavioral Effects of Post-weaning Social Isolation in Males and Females. Front. Behav. Neurosci. *13*, 66.
44. Martel, J.C., and Gatti McArthur, S. (2020). Dopamine Receptor Subtypes, Physiology and Pharmacology: New Ligands and Concepts in Schizophrenia. Front. Pharmacol. *11*, 1003.
45. Kritzer, M.F., and Creutz, L.M. (2008). Region and sex differences in constituent dopamine neurons and immunoreactivity for intracellular estrogen and androgen receptors in mesocortical projections in rats. J. Neurosci. *28*, 9525–9535.
46. Walker, Q.D., Rooney, M.B., Wightman, R.M., and Kuhn, C.M. (2000). Dopamine release and uptake are greater in female than male rat striatum as measured by fast cyclic voltammetry. Neuroscience *95*, 1061–1070.
47. Zachry, J.E., Nolan, S.O., Brady, L.J., Kelly, S.J., Siciliano, C.A., and Calipari, E.S. (2021). Sex differences in dopamine release regulation in the striatum. Neuropsychopharmacology *46*, 491–499.
48. Uchida, K., Otsuka, H., Morishita, M., Tsukahara, S., Sato, T., Sakimura, K., and Itoi, K. (2019). Female-biased sexual dimorphism of corticotropin-releasing factor neurons in the bed nucleus of the stria terminalis. Biol. Sex Differ. *10*, 6.
49. Whylings, J., Rigney, N., Peters, N.V., de Vries, G.J., and Petrulis, A. (2020). Sexually dimorphic role of BNST vasopressin cells in sickness and social behavior in male and female mice. Brain Behav. Immun. *83*, 68–77.
50. Murínová, J., Hlaváčová, N., Chmelová, M., and Riečanský, I. (2017). The Evidence for Altered BDNF Expression in the Brain of Rats Reared or Housed in Social Isolation: A Systematic Review. Front. Behav. Neurosci. *11*, 101.
51. Yu, Y., Shu, Y., and McCormick, D.A. (2008). Cortical action potential backpropagation explains spike threshold variability and rapid-onset kinetics. J. Neurosci. *28*, 7260–7272.
52. Hammack, S.E., Mania, I., and Rainnie, D.G. (2007). Differential expression of intrinsic membrane currents in defined cell types of the anterolateral bed nucleus of the stria terminalis. J. Neurophysiol. *98*, 638–656.
53. Rodríguez-Sierra, O.E., Turesson, H.K., and Pare, D. (2013). Contrasting distribution of physiological cell types in different regions of the bed nucleus of the stria terminalis. J. Neurophysiol. *110*, 2037–2049.

STAR★METHODS

KEY RESOURCES TABLE

REAGENT or RESOURCE	SOURCE	IDENTIFIER
Antibodies		
Chicken polyclonal anti-GFP	ABCAM	Cat# ab13970; RRID: AB_300798
Goat-*anti*-chicken,Alexa Fluor 488	Jackson ImmunoResearch Laboratories	Cat# 103-545-155; RRID: AB_2337390
Rabbit polyclonal anti-dsRed	Takara Bio	Cat# 632496; RRID: AB_10013483
Goat-*anti*-rabbit, Alexa Fluor 568	Life Technologies Co.	Cat# A11011; RRID: AB_143157
Bacterial and virus strains		
AAV2/9-EF1a-DIO-EYFP-WPRE-HGHpA	Shanghai Taitool Bioscience Co., Ltd.	Cat# S0178-9-H20
AAV2/9-hSyn-DIO-hM3D(Gq)-mCherry-WPRE-pA	Shanghai Taitool Bioscience Co., Ltd.	Cat# S0192-9
AAV2/9-hSyn-DIO-mCherry-WPRE-pA	Shanghai Taitool Bioscience Co., Ltd.	Cat# S0240-9
AAV2/9-EF1a-DIO-Kir4.1-eGFP-WPRE-HGHpA	Shanghai Taitool Bioscience Co., Ltd.	Cat# S0454-9-H50
AAV2/9-hEF1a-DIO-EGFP-WPRE-pA	Shanghai Taitool Bioscience Co., Ltd.	Cat# S0270-9
AAV2/9-hSyn-FLEX-mCherry-2A-TVA-2A-RvG-WPRE-pA	Shanghai Taitool Bioscience Co., Ltd.	Cat# S0380-9
RV-ENVA-ΔG-EGFP	Brain VTA [Wuhan] Co., Ltd.	Cat# R01001
Chemicals, peptides, and recombinant proteins		
TTX	Tocris	Cat# 1078/1
AP5	Tocris	Cat# 0106/10
Bicuculline	Tocris	Cat# 2503/10
CNQX	Sigma-Aldrich	C127-5MG
Clozapine-N-oxide	ENZO	Cat# BML-NS105-0025
DAPI	CST	Cat# 4083S
ProLong Gold	Life Technologies Co.	Cat# P36930
Critical commercial assays		
ELISA	Shanghai Univ-biotechnology Co., Ltd.	N/A
Experimental models: Organisms/strains		
Rat: Sprague Dawley (SD)	Slac Laboratory Animal	N/A
Rat: Drd1-Cre	Beijing Biocytogen Co., Ltd.	N/A
Rat: Drd2-cre	Beijing Biocytogen Co., Ltd.	N/A
Oligonucleotides		
probe-CRE-C1	ACD	Cat# 312281
Rn-Drd1a-C2	ACD	Cat# 317031-C2
Rn-Drd2-C3	ACD	Cat# 315641-C3
Software and algorithms		
MATLAB	MathWorks	N/A
Adobe Illustrator CC	Adobe	N/A
ImageJ	NIH	N/A
GraphPad Prism 8	GraphPad	N/A
Clampfit 10.7	Molecular Devices Co.	N/A
Mini Analysis	Synaptosoft	N/A
Other		
Digidata 1332	Axon	N/A
MultiClamp 700B	Axon	N/A

RESOURCE AVAILABILITY

Lead contact

Further information and requests for resources and reagents should be directed to the Lead Contact, Zuo-Ren Wang (zuorenwang@ion.ac.cn).

Materials availability

This study did not generate new unique reagents.

Data and code availability

All data are available upon request from the lead contact. This paper does not report original code. Any additional information required to reanalyze the data reported in this work paper is available from the lead contact upon request.

EXPERIMENTAL MODEL AND SUBJECT DETAILS

Wild-type (male and female), Drd1::Cre (male), and Drd2::Cre (male and female) transgenic SD rats were used in this study. Wild-type SD rats, aged three weeks, were purchased from Shanghai SLAC Laboratory Animal Co., Ltd. The Drd1::Cre and Drd2::Cre transgenic rats were generated by Beijing Biocytogen Co., Ltd. At postnatal day 21 (P21), rats were divided into group-housed or single-housed groups, according to experimental needs. Rats were reared following a standard 12 h light/dark cycle (lights on at 07:00). Water and food were supplied *ad libitum*. All animals were used and operated on in accordance with the regulations of the Institutional Animal Care and Use Committee of the Center for Excellence in Brain Science and Intelligent Technology of the Chinese Academy of Sciences.

METHOD DETAILS

PWSI modeling procedure

Rats were normally reared for the first three weeks and then randomly assigned to the experimental or control group at P21. Rats in the experimental group (PWSI) were single-housed separately, while rats in the control group were group-housed (GH; 2–3 rats per cage). The PWSI procedure was completed when the rats in both groups were aged 8 weeks. During the PWSI process, aside from the necessary provision of water and food, contact between rats and feeders was reduced as much as possible. Behavioral tests, measurement of corticosterone, and patch-clamp recordings were performed after the PWSI model was established. The PWSI rats in our experiments were maintained in a socially isolated state during the whole behavioral test periods.

Behavioral tests

Before behavioral tests, each rat was handled for 5–10 min at a time, twice a day, for a total of two days. The behavioral tests in our experiment were performed sequentially with an interval of one day. In the chemogenetic manipulation experiments, rats expressing human muscarinic receptor 3 (hM3D) and mCherry were intraperitoneally injected with clozapine-N-oxide dihydrochloride (CNO, 3 mg/kg, ENZO Life Sciences) 30 min before the behavioral tests. All of the virus expression sites were validated *post hoc* after behavioral tests. In the pharmacological manipulation experiments, rats with abnormal motor responses after cannula implementation were excluded. For the intra-dBNST infusion of quinpirole (D2 agonist, MedChemExpress), 500 nL quinpirole (1 μg/μL) was infused to each side of the dBNST within 5 min. Five minutes after removing the injection tube, behavioral tests were performed. Quinpirole or saline was randomly administered to rats of the same batch in a counter-balanced manner in the behavioral tests. For all behavioral tests, we used Noldus EthoVision (Noldus Information Technology, Netherlands) to track the center of gravity of rats to acquire the specific parameters of each behavioral test.

Open field test (OFT)

The open field arena measured 60 cm × 60 cm × 45 cm. The central area was 900 cm^2. In the OFT, the locomotion distance, number of center entries, and total time that rats spent in the center zone were analyzed. The entire test lasted 15 min.

Elevated plus maze (EPM) test

The EPM was fixed on a cross platform 54 cm above the ground. Each arm measured 50 cm × 10 cm. One of the two pairs of opposite arms was closed by a wall, and the other was open. The height of the wall was 40 cm. At the beginning of the test, rats were first placed at the distal end of an open arm, facing away from the center of the elevated plus maze. Video recording was started when the center of gravity of the rat entered the central zone, and the test ended 10 min later. In this test, the number of entries into the open arms, the duration spent in each arm, and the total distance traveled in the EPM were analyzed.

Light-dark box test (L-D box)

The L-D box consisted of two chambers, one of which was a large chamber with a lid and the other a small chamber without a lid. The dark and light boxes measured 30 cm × 30 cm × 30 cm and 20 cm × 30 cm × 30 cm, respectively. There was a small opening

(10 cm × 10 cm) between the two chambers. In this test, activity was recorded for 10 min after rats were placed in the light box, and the duration spent in the light box was measured to reflect the anxiety level of the rats.

Forced swim test (FST)

The FST is used as a measurement of depression-like behavior in mice. In this test, the time that mice spend floating on water without struggling reflects passive coping. However, we observed the movement of rats (SD rats) in water in containers of different sizes and found that each rat kept swimming for different durations and would sink into the water if they stopped swimming. Thus, we used the total distance the rats swam in the water as an index of passive coping of SD rats. The container used for the FST was a cylinder with a diameter of 30 cm, and the wall height was 50 cm. During the test, the water level was adjusted to approximately 40 cm high, and the temperature was set to 25°C. The whole test lasted for 6 min, and the data from 3 to 6 min were analyzed.

Three-chamber social preference test (SPT)

The SPT was used to examine the sociality of rats. Rats were placed on one side of a lidless rectangular box, and a toy rat was placed on the other side as an exploration object for the subjects. The three-chambered box measured 90 cm × 45 cm × 30 cm, with 30 cm × 45 cm × 30 cm for each chamber. The SPT was divided into two sessions, and each session lasted for 10 min. In the first session, two empty cages were placed on both sides of the test box to allow the subjects to adapt to the context. In the second session, a live rat or a toy rat was randomly placed in the cages on both sides of the box. Rats placed within the cage in the box had acclimated to the cage for 4–5 min one day before testing to reduce their stress response. Rats were placed in the middle zone of three-chambered box at the beginning of the test. Then, their exploratory activities were immediately recorded. The total duration subjects spent exploring the rat and toy sides was calculated. In addition, the ratio of social preference was calculated as (time spent on the rat side − time spent on the toy rat side)/(time spent on the rat side + time spent on the toy rat side) × 100%.

Measurement of corticosterone

An enzyme-linked immunosorbent assay (ELISA) was used to measure the serum concentration of corticosterone in group-housed (GH) and PWSI rats. Approximately 1.6–1.7 mL of blood was collected from each rat. After standing for 2 h, the collected whole blood was centrifuged at 4°C and 2000 g for 20 min, and supernatant was extracted. Measurement of serum corticosterone concentration was performed by Shanghai Univ-biotechnology Co., Ltd.

Electrophysiology

The solution formulations for *in vitro* electrophysiological recordings were as follows: artificial cerebrospinal fluid (ACSF) contained (in mM) NaCl 118, KCl 2.5, glucose 10, $NaHCO_3$ 26, NaH_2PO_4 1, $CaCl_2$ 4, and $MgCl_2$ 4. Cutting solution contained (in mM) NMDG 90, KCl 2.5, NaH_2PO_4 1.2, $NaHCO_3$ 30, HEPES 20, D-glucose 25, sodium ascorbate 5, thiourea 2, sodium pyruvate 3, NAC 5, $MgSO_4 \cdot 7H_2O$ and $CaCl_2$ 0.5. ACSF and cutting solution was adjusted to PH 7.3, 290 mOsm, and internal solution to PH 7.3, 275 mOsm.

High-potassium internal solution (K^+) contained (in mM) K-gluoconate 126, HEPES 10, KCl 2, $MgCl_2$ 2, Na_2ATP 4, Na_3GTP 0.4, EGTA 0.2, and creatine phosphate 10; high-cesium internal solution (Cs^+) contained (in mM) $CsMeSO_4$ 130, HEPES 10, CsCl 5, MgATP 4, Na_3GTP 0.3, EGTA 0.5, and creatine phosphate 10. High-cesium internal solution was used for recording mEPSCs and mIPSCs.

Rats weighing 350–450 g were anesthetized and perfused with ice-cold cutting solution. Then, rats were decapitated, and brain tissue was placed into an ice-cold slicing solution. Brain tissue was cut into 350 μm-thick slices using a Leica VT1200S vibratory slicer. The brain slice was kept at room temperature (25°C) ACSF for ~1 h before use. All solutions above were oxygen-saturated solutions, and brain slices were recorded at 32°C. Electrophysiological signals were sampled at 10 kHz by an analog-to-digital converter (Digidata 1332) and were low-pass filtered at 2 kHz. Samples with Ra of less than 25 MΩ and holding current of less than 100 pA were analyzed. The analysis of electrophysiological recording data was performed using Clampfit 10.7 (Molecular Devices Co.), Mini Analysis (Synaptosoft), and MATLAB software.

In the threshold measurement experiment, the amplitude of the action potential was recorded by whole-cell patch-clamp recording, with neurons recorded in a current clamp configuration. Then, a series of depolarized step currents (−10 pA–220 pA), with a duration of 500 ms, was injected into the neuron in a current clamp mode to induce an action potential. In the measurement of neuronal electrophysiological response type, the range of depolarization step currents was −100 pA to 150 pA. In the experiment measuring input resistance (Rin), neurons were also recorded in current clamp configuration. Then, the cell was stimulated with an outward current of −20 pA for a duration of 500 ms to hyperpolarize the membrane potential, and changes in the membrane potential were recorded. Hyperpolarization stimuli were repeated 10 times. In order to calculate the R_{in}, mean membrane potentials of 100 ms before and after the stimuli were used ($R_{in} = \Delta V/\Delta I$). The mean values of membrane potentials within the 100 ms period before the first sweep stimulation in the recorded data of each cell were taken as the value of the resting membrane potential (RMP). The action potential threshold was identified by finding the point in the rising stage of first action potential of the first sweep, which showed that $\Delta V/\Delta I$ = 20 v/s was the action potential threshold.[51]

For classifying the different types of dBNST $Drd1^+$ and $Drd2^+$ neurons based on their electrophysiological properties, the responses to a gradient depolarizing and hyperpolarizing current injection were used as the standard.[52,53] Low-threshold bursting (LTB) neurons exhibited a depolarizing sag in the condition of hyperpolarization and a rebound spike on the offset of hyperpolarized

current injection. In the depolarization condition, even though LTB neurons exhibited an initial burst of spikes, the following traces showed a regular spike pattern. Regular spiking (RS) neurons exhibited a depolarizing sag in the condition of hyperpolarization; however, they did not have a burst of rebound spikes on the offset of hyperpolarized current injection. Neurons with fast inward rectifying K^+ conductance (fIR) showed fast anomalous rectification in the condition of gradient hyperpolarizing current injection. Late-firing neurons exhibited a long latency to burst spikes in the condition of depolarized current injection. Spontaneously active (SA) neurons exhibited spontaneous bursting of spikes without depolarized current injection.

In the miniature excitatory postsynaptic current (mEPSC) recording experiment, Cs^+ internal solution was used, and mEPSCs were recorded in the voltage clamp configuration. The membrane potential was held at −70 mV during recording, and TTX (0.5 μM), AP-5 (50 μM, NMDA receptor antagonist), and bicuculline (10 μM, GABA-A receptor antagonist) were applied into ACSF. In the miniature inhibitory postsynaptic current (mIPSC) recording experiment, Cs^+ internal solution was used, and the membrane potential was held at 0 mV in the voltage clamp configuration. TTX (0.5 μM) and CNQX (10 μM, AMPA receptor antagonist) were applied into ACSF. Each cell was recorded for 20–30 sweeps, with each sweep lasting for 10 s. The frequency and amplitude of mEPSCs and mIPSCs were analyzed using Mini Analysis software.

In the experiment of functional validation of the chemogenetic system, the response of hM3D-expressed $Drd2^+$ neurons to clozapine-N-oxide dihydrochloride (CNO) in the dBNST was examined. In detail, cells were recorded under a current clamp configuration, and then CNO (10 μM) was applied into the ACSF. Changes in membrane potentials and action potentials before and after CNO application were analyzed.

Viruses

The viruses and their titers were as follows: AAV2/9-EF1a-DIO-EYFP-WPRE-HGHpA = 1.15×10^{13}, AAV2/9-hSyn-DIO-hM3D(Gq)-mCherry-WPRE-pA = 1.70×10^{13}, AAV2/9-hSyn-DIO-mCherry-WPRE-pA = 1.13×10^{13}, AAV2/9-EF1a-DIO-Kir4.1-eGFP-WPRE-HGHpA = 2.21×10^{13}, AAV2/9-hEF1a-DIO-EGFP-WPRE-pA = 1.78×10^{13}, AAV2/9-hSyn-FLEX-mCherry-2A-TVA-2A-RvG-WPRE-pA = 4.58×10^{12}, and RV-ENVA-ΔG-EGFP = 2.00×10^{8}. All of the viruses were purchased from Shanghai Taitool Bioscience Co., Ltd., except the RV-ENVA-ΔG-EGFP (Brain VTA [Wuhan] Co., Ltd.).

Stereotaxic surgery and microinjection

Rats were anesthetized with isoflurane. The position coordinates used to determine the location of the dBNST were AP −0.2 mm, ML ± 1.3 mm, and DV 5.9 mm. The injection volume of virus was 0.3 μL, with the exception of 1 μL for AAV2/9-EF1a-DIO-EYFP-WPRE-HGHpA. After surgery, rats recovered for 2 weeks before behavioral tests. In the retrograde tracing experiment, the AAV2/9-hSyn-FLEX-mCherry-2A-TVA-2A-RvG-WPRE-pA was first unilaterally injected into dBNST at P64, and then the RV-ENVA-ΔG-EGFP was also injected dBNST at P78. After one week's expression of RV-ENVA-ΔG-EGFP, the brain tissue was collected for microscopic observation. In the pharmacological experiments, quinpirole was injected into the dBNST via a cannula (RWD Life Science, China), followed by the behavioral tests. The cannula implantation procedure was similar to the virus injection procedure, except that the tip of the cannula was placed 0.15 mm above the dBNST region. Three nails were first immobilized on the skull, then the dental cement was used to secure the cannula on the skull. After surgery, rats were returned to their cages and allowed to recover for one week before drug administration and behavioral tests.

Immunohistology and imaging

First, brain slices were soaked in phosphate buffer solution (PBS; 5 min, twice), and then DAPI (1:1000; CST, #4083S) was added. After 5 min, slices were washed with PBS to remove DAPI (5 min, twice) and then mounted with 75% glycerin. Brain slices were then imaged using an Olympus VS.120 high-through fluorescence microscopic imaging system (10× air objective).

To verify the expression specificity of AAV2/9-EF1a-DIO-EYFP-WPRE-HGHpA, we performed an *in situ* hybridization and immunohistochemistry experiment. For the *in situ* hybridization experiment (RNAscope), the protocol provided by the manufacturer was followed. Probes were purchased from Advanced Cell Diagnostics, USA. The probes used in this study were as follows: probe-CRE-C1 (#312281), Rn-Drd1a-C2 (#317031-C2), and Rn-Drd2-C3 (#315641-C3). For the immunohistochemistry experiment, slices were first incubated in 2.5% BSA (PBS; Sigma, #V900933-100G) solution at room temperature for 1 h, and then primary antibody (chicken polyclonal anti-GFP, ABCAM, #ab13970 or rabbit polyclonal anti-dsRed, Takara Bio, #632496; 1.25% BSA, 1:500) was applied and incubated with the sections at 4°C overnight. Secondary antibody (goat-*anti*-chicken, Alexa Fluor 488, Jackson ImmunoResearch Laboratories, #103-545-155 or Goat-*anti*-rabbit, Alexa Fluor 568, Life Technologies Co., #A11011) in 1.25% BSA was applied for 2 h at room temperature. After two PBS washes (15 min per wash), the sections were mounted for imaging using anti-fade reagent (Life Technologies Co., #P36930). Sections obtained after RNAscope and immunohistochemistry were imaged using an Olympus FV3000 laser scanning confocal microscope.

QUANTIFICATION AND STATISTICAL ANALYSIS

Quantification of immunofluorescence

Quantification of immunofluorescence (EYFP, mCherry, EGFP and mRNA) was performed by using ImageJ. For each animal, 3 sections randomly selected from dBNST were used to quantify the expression of corresponding fluorescence protein or mRNA.

Quantification of retrograde labeling

To quantify the input of dBNST Drd1$^+$ and Drd2$^+$ neurons, the serial coronal brain slices of 50 mm thickness were imaged using an Olympus VS.120 high-through fluorescence microscopic imaging system (10× air objective). The retrograded GFP$^+$ neurons of region of interests were manually counted. The input of dBNST Drd1$^+$ and Drd2$^+$ neurons were normalized by the number of starter cell (both express GFP and mCherry) in dBNST of each animal.

Statistics

For comparisons between two groups, Student's *t* test or the Mann-Whitney *U* test was used. The criterion for selection of the statistical method was that, if the sample number from both groups was less than 20, a normality test was performed first. In sample numbers from two groups, where both met the assumption of normality, Student's *t* test was used. Otherwise, the Mann-Whitney *U* test was used. However, if the sample number of one group was greater than 20, Student's *t* test was used without a normality test. Unpaired and two-tailed Student's *t* tests were used for all statistical analyses, with the exception of paired and two-tailed tests used for the results of the effects of the CNO and quinpirole on neuronal excitability. A two-way analysis of variance (ANOVA) with Bonferroni correction was used to analyze the effect of step-current injection on the action potential numbers of neurons in two groups.